NUREG/CR-4078

Program for Field Validation of the Synthetic Aperture Focusing Technique for Ultrasonic Testing (SAFT UT)

Final Report

Prepared by D. R. Hamlin

Southwest Research Institute

Prepared for
U.S. Nuclear Regulatory Commission

NUREG/CR-4078
SwRI Project 17-5023
R5

Program for Field Validation of the Synthetic Aperture Focusing Technique for Ultrasonic Testing (SAFT UT)

Final Report

Manuscript Completed: October 1984
Date Published: November 1985

Prepared by
D. R. Hamlin

Southwest Research Institute
P. O. Drawer 28510
6220 Culebra Road
San Antonio, TX 78284

Prepared for
Division of Engineering Technology
Office of Nuclear Regulatory Research
U.S. Nuclear Regulatory Commission
Washington, D.C. 20555
NRC FIN B5605

ABSTRACT

This final report describes work performed by Southwest Research Institute for the Nuclear Regulatory Commission (NRC) in fulfillment of NRC Contract No. NRC-04-77-145: "Program for Field Validation of the Synthetic Aperture Focusing Technique for Ultrasonic Testing (SAFT UT)."

The purpose of the project was to validate the effectiveness of SAFT UT as a nondestructive examination technique for nuclear power and other related industries. SAFT UT is an ultrasonic imaging method for accurate measurement of the spatial location and extent of acoustically reflective surfaces (flaws) contained in objects such as structural components and weldments in nuclear power reactor systems. The increased measurement accuracy offered by SAFT, when compared with that provided by measurement methods now in use, will improve the reliability of flaw severity assessment with resultant safety and economic benefits to the nuclear power industry.

This report presents a comprehensive discussion of the work accomplished in evaluating the performance capabilities of the developed SAFT UT inspection system. Inspection results obtained using both 0-degree longitudinal and angle-beam operating modes are presented. These results include laboratory and nuclear power plant field site examinations on a variety of defect types contained within carbon and stainless steel flat plate and cylindrical test specimens or components. The SAFT UT processed data flaw images are evaluated by comparing them to results obtained from destructive sectioning of [illegible]sing flaw fabrication data which predicted actual flaw depth, orientation and size. On the basis of these evaluations, conclusions are presented which summarize the performance capabilities of the SAFT UT inspection technique.

EXECUTIVE SUMMARY

The economics and safety of the nuclear power industry will be improved by perfection of an ultrasonic (UT) examination method having sensitivity and reliability greater than that exhibited by conventional UT. Research has shown that a new UT method known as the Synthetic Aperture Focusing Technique for Ultrasonic Testing (SAFT UT) has high potential for supplying the needed improvement. The purpose of the subject work was to engineer and build a practical SAFT UT system to: (1) measure its performance in examining test specimens that realistically simulate actual components used in nuclear power reactor pressure vessels and related components and, (2) perform an examination at a nuclear power plant field site using the system.

Details of the SAFT UT system hardware specifications, processing algorithms, cathode-ray tube color image presentations, and operational procedures have been discussed in previous reports (1).

This report describes results of performance evaluation tests obtained using two different types of inspection modes. These were the 0-degree longitudinal focused beam inspection mode and the longitudinal angle-beam surface contact inspection mode. All of the 0-degree inspection mode examinations were performed first and these results are presented in Sections 5 and 6. These tests were performed using a 5-megahertz focused beam transducer having a diameter of 0.75 inch and a 3-inch focal length. Following these tests, all of the longitudinal mode angle-beam surface contact inspection mode examinations were performed and these results are presented in Sections 7 through 10. These tests were performed using a 3-megahertz round transducer having a 0.375-inch diameter. The transducer was mounted on a shoe which tracked the inspection surface of the component being examined. In all of these tests (both 0-degree and angle-beam), the SAFT examination system could be programmed to use different sized synthetic apertures and was operated on curved and/or irregular surfaces typical of industrial components. Near the end of the project the system was used to perform a nuclear power plant field site examination and these results are presented in Section 11.

This project successfully demonstrated that SAFT UT can perform UT examinations under realistic conditions with much better accuracy and sensitivity than can conventional methods and equipment. Lateral resolution of 1 to 2 wavelengths (0.05 to 0.1 inch with the 5-megahertz transducer and 0.076 to 0.152 inch with the 3-megahertz transducer), range resolution of 1 wavelength, and image signal-to-noise ratios of 20 to 40 dB were routinely achieved. These results are in good agreement with analytical predictions and verify parameter selection and equipment operation.

Image interpretation proved to be much easier, quicker, and more reliable than interpretation of indications produced by conventional UT equipment. These results are important and are emphasized. There was not a single incident in which operators misinterpreted an image feature as being produced by a flaw when, in fact, no flaw was present. Also, operators could be quickly trained to interpret images reliably even when they had no previous interpretive experience using conventional UT equipment.

A simple calibration procedure was devised and used throughout the test program with good results. This procedure is very unusual in that no machined reference reflector was required nor used. Instead, operators adjusted the instrumentation gain based on visual observation of unprocessed signals detected from the volume to be imaged. To a reader experienced with calibration of conventional equipment, such a method will appear to be subjective and unreliable. We have found, however, that the method worked very consistently. Not a single instance occurred in which results of image interpretation would have been improved by calibrating differently. Even though this calibration method gave accurate results consistently, final endorsement should be withheld pending accumulation of a larger statistical base of experience.

In the reported tests, the sensitivity of SAFT UT was higher than the sensitivity of conventional equipment calibrated by normal procedures. The amount of improvement has not been quantified; but, for two tests, it was estimated to be between 10 and 20 dB. However, the higher sensitivity did not result in an overstatement of flaw size nor in an improper conclusion of the presence of flaws where none existed.

As a result of the tests and subsequent evaluations performed during this program, the following conclusions can be made regarding the performance of the SAFT UT inspection capability:

(1) SAFT UT is a viable nondestructive evaluation technique and is capable of performing accurate measurements of the spatial location and extent of acoustically reflective surfaces contained in objects similar to the structural components and weldments in nuclear power reactor systems.

(2) SAFT UT inspection equipment demonstrated effective operation at higher sensitivity levels than is practical using conventional UT inspection equipment.

(3) Interpretation of the SAFT UT image display is much more definitive and easier to perform than evaluation of indications obtained from conventional UT equipment.

(4) The SAFT UT technique is subject to beam angle and orientation constraints (as is any ultrasonic technique). For this reason, a general purpose SAFT UT inspection system must be capable of operating at a variety of beam angles and orientations. The purpose in providing this type of flexibility is to increase the probability of receiving some of the transmitted acoustic energy by favorably orienting the sound beam in relationship to the reflecting surface of the defect to be imaged.

(5) The SAFT UT technique can be effectively implemented using either focused beam or surface contact inspection modes. Both of these techniques are applicable to surfaces geometry typically encountered in nuclear power plant reactor vessel and piping systems.

(6) To obtain high quality images of certain vertically oriented flaws, additional research is needed in defining the physics of the acoustic interactions that take place at the flaw surface. The SAFT UT system's capability to provide better flaw images is currently constrained by acoustic considerations, not by the SAFT processing technique.

TABLE OF CONTENTS

TABLE OF CONTENTS (Cont'd)

LIST OF ILLUSTRATIONS

LIST OF ILLUSTRATIONS (Cont'd)

LIST OF ILLUSTRATIONS (Cont'd)

LIST OF ILLUSTRATIONS (Cont'd)

LIST OF ILLUSTRATIONS (Cont'd)

LIST OF ILLUSTRATIONS (Cont'd)

LIST OF ILLUSTRATIONS (Cont'd)

LIST OF ILLUSTRATIONS (Cont'd)

1. INTRODUCTION

Southwest Research Institute (SwRI) has completed a project entitled "Program for Field Validation of the Synthetic Aperture Focusing Technique for Ultrasonic Testing (SAFT UT)." The project's purpose was to continue the development of SAFT UT and to validate its usefulness for inservice inspection applications. SAFT UT is an ultrasonic imaging method for accurately measuring the spatial locations and extent of flaws contained in objects such as structural components and weldments in nuclear power reactor systems. The increased measurement accuracy offered by SAFT UT, when compared with that provided by measurement methods now in use, will improve the reliability of flaw severity assessment with resultant safety and economic benefits to the nuclear power industry.

This project was part of a team effort being conducted by the University of Michigan (U of M) and SwRI. Although the two groups worked under separate contracts, their efforts were integrated and synergetic. The U of M group was responsible for studying the theoretical and long-range design aspects of SAFT UT while SwRI, working with information and advice supplied by U of M, contributed the engineering and performance evaluations necessary to produce and validate a practical field tool.

The objectives of this program were to:

- Produce a SAFT UT system in a form useful for field test.
- Validate the performance of that system for characterizing both real and simulated flaws in realistic test specimens.
- Conduct a field trial using the system on an actual structure.
- Estimate the reliability and confidence level for SAFT UT examinations and compare those results with similar estimates made for conventional ultrasonic methods.

The ultimate goal was to produce a field-rated system for highly accurate flaw size measurements and to conduct sufficient testing of that system to promote its acceptance by industrial and regulatory authorities.

This report presents the result of work accomplished in defining the performance capabilities of SAFT UT which serve to successfully demonstrate the applicability of this technique for use in performing the inspection of nuclear power plant reactor vessel and piping components.

2. EVALUATION OF SYSTEM PERFORMANCE CAPABILITY

Details of the SAFT UT system hardware specifications, processing algorithms, image display presentations, and operational procedures have been discussed in previous reports (1). The SAFT UT inspection system performance capability has been evaluated using results obtained from a variety of defect types contained in the following test specimens:

- Butt welded carbon steel plate containing weld fabrication flaws.
- A series of stainless steel test plates containing weld fabrication flaws.
- A Duane Arnold safe-end pipe section containing an intergranular stress corrosion crack (IGSCC) defect.
- A cylindrical stainless steel pipe specimen containing several IGSCC defects.
- A set of clad carbon steel plates containing buried vertically oriented fatigue cracks.
- A centrifugally cast stainless steel specimen containing machined reflectors.

These specimens contained defects representative of both volumetric and crack type flaws at varying through-wall depths, sizes, and orientations. The defect types evaluated included:

- Porosity
- Slag
- Heat-affected zone cracks
- IGSCC defects
- Vertically oriented fatigue cracks (buried underclad)
- Lack of penetration flaw
- Lack of fusion flaw

Results from the butt welded carbon steel plate were evaluated using comparison to destructive sectioning data. The Duane Arnold safe-end specimen results were evaluated using data from previously published reports (2). The series of stainless steel test plates were evaluated in blind tests. These results are published here so that they may be compared to future destructive sectioning results. The remainder of the results were evaluated using flaw fabrication data which reliably estimated the flaw depth, length, through-wall extent, orientation, and shape.

3. ADJUSTMENT OF SYSTEM SENSITIVITY (EQUIPMENT CALIBRATION)

3.1 Introduction

As with any nondestructive evaluation (NDE) instrument system, a methodology is needed to guide SAFT UT operators in their adjustment of equipment sensitivity. Since operational procedures and measurement resolution of SAFT UT differ greatly from those of conventional UT equipment, it is questionable whether calibration procedures recommended in Section XI of the American Society of Mechanical Engineers (ASME) Code for conventional equipment are necessarily appropriate or optimum for SAFT UT. Therefore, a specific goal for this program was to develop equipment adjustment procedures complementing the unique measurement capabilities of SAFT UT. This goal was accomplished, and results are described in this section.

3.2 Background

The primary deficiency of conventional UT equipment is a lack of spatial resolution, especially lateral resolution. This deficiency creates the opportunity for signals produced from multiple, separate regions (reflectors) to coexist, and operators are presented with a very difficult (sometimes impossible) task to reliably interpret the composite indications. The difficulty in interpretation increases rapidly as the analysis threshold is lowered because it forces the operator to consider and interpret a larger number of indications.

These obstacles are widely recognized, and inspection procedures and regulatory guidelines have been designed to minimize the interpretation problems resulting from poor spatial resolution. Since interpretation difficulty is a very sensitive function of analysis threshold, conventional UT examination procedures are designed to allow the use of relatively high analysis thresholds. As a direct result, most current examination procedures call for use of both multiple examination angles and directions in an attempt to detect a strong indication from flaws having any orientation. While these procedures are definitely helpful in compensating for the deficiencies of conventional UT equipment, there is general consensus in the NDE community that inspection reliability could be improved if a practical method permitting lower analysis thresholds could be found.

Such a method is not yet in general use, however, and calibration and analysis procedures currently employ high analysis thresholds, which may result in relatively low inspection sensitivity.

3.3 Adjustment of Sensitivity for SAFT UT

Because of the excellent resolution inherent in the SAFT method, its images are interpreted on the basis of identifying image patterns that are characteristic of flaws and flaw boundaries. For a given flaw size, these characteristic patterns are much more definitive and easier to interpret than are indications obtained from conventional equipment. Because of improved interpretability, it is practical to increase inspection sensitivity by adjusting SAFT to have a high gain and low analysis threshold. However, while such adjustments are desired, practical considerations do place limits on the maximum usable instrumentation gain; and image clarity may suffer if these limits

are exceeded. Compliance with these limits form the basis of the calibration procedure devised and followed during these studies.

The practical limit on instrumentation gain is because of the need to avoid nonlinear amplification (caused from overload of the amplifiers) of the largest signal returning from the volume to be imaged. It is known that nonlinear signals can cause increased sidelobes and background clutter, both of which decrease the sensitivity associated with the image. Future technical developments may reduce or overcome the degradation resulting from nonlinear signals, but presently it is prudent to adjust instrumentation gain to prevent nonlinearity.

The calibration procedure used in these studies is simply, first, to identify the largest signals arriving from the region to be imaged and then to increase the gain to the threshold of signal nonlinearity. Such adjustment optimizes the dynamic range of subsequent images and, therefore, maximizes the sensitivity of inspection.

In practice, use of this calibration procedure has b n very satisfactory. Image signal-to-noise ratio is consistantly better than 20 dB, which allows detection and sizing of weak reflectors even when they are near larger, more reflective flaws. In fact, for several tests in which flaw indications were below the recording threshold using conventional procedures, clear images permitting accurate flaw characterization were produced by adjusting the SAFT UT according to the procedure just described. Operation at the higher sensitivity did not result in an overstatement of flaw size nor in an improper conclusion of the presence of flaws where none existed.

4. DETERMINATION OF LOCATION AND SIZING ACCURACIES

4.1 Image Interpretation Overview

Determining the spatial location and extent of a flaw is accomplished by evaluating the information presented in a series of operator-selected cathode-ray tube (CRT) color image displays. The image reconstruction algorithm permits the system operator to specify parameters that define the volumetric region in which imaging is to be performed (1). The volumetric region is subdivided into pixels (cells) upon which the reconstruction algorithm operates using the ultrasonic test data obtained during scanning. Upon completion of processing, every cell in the volumetric region contains an amplitude value representing that cell's contribution to the reconstructed image. The final image is formed by displaying the computed signal amplitude as a function of cell location within the volume. The image is then interpreted by noting the locations of locally high signal amplitude. It should be noted that the reconstruction algorithm does not attempt to directly determine the size and location of the defect. The location and size are deduced by operators from the patterns formed by cells that show evidence of containing a defect.

4.2 Image Interpretation Considerations

Recognizing flaws contained within image displays depends on operator interpretation of cell patterns containing amplitude information. Modulation of image color according to signal amplitude using a suitably designed color scale (1) simplifies the recognition task by accentuating regions containing higher amplitudes. Accentuation is accomplished by using a "rainbow" type color sequence in which low amplitudes are assigned to blue or "cool" colors and progressively higher amplitudes are assigned to green, yellow, orange, and red colors. Defects are then represented as a collection of brightly colored cells displayed against a background of subdued colors. This presentation format permits a trained operator to readily identify potentially interesting regions of the image being displayed. Because of the system's sensitivity-adjustment procedure used in performing examinations, the patterns formed by the collection of higher amplitude cells will define the flaws contained within the imaged volume. The spatial location of these patterns (flaws) are described with high accuracy by the coordinates used during image reconstruction. Determination of the spatial size requires a procedure for defining the pattern boundaries. The accuracy with which the flaw boundaries can be judged constitutes the lateral and axial resolution performance capability of the system.

4.3 Technique for Determining Flaw Size

A sizing technique was defined for the SAFT UT reconstructed images by comparing them to the examined flaw surface from which they were obtained. This was accomplished by destructive sectioning of several volumetric and crack-type flaws contained in a 4-inch (102-mm) thick butt-welded carbon steel

plate. The evaluation indicated that by analyzing the surface-spread function* at selected locations of the image's cell pattern representing the flaw surface, boundary locations can be determined. The accuracy of this determination is a function of the amplitude threshold value used.

Because of limitations on the measurement accuracies achieved during destructive sectioning, it was unrealistic to attempt to define boundary location accuracies of less than one wavelength. Evaluation of the surface-spread functions on the destructively sectioned flaws indicates that boundary locations accurate to within 1 wavelength can be obtained using an amplitude threshold that is 8 dB down from the maximum normalized flaw amplitude. Using this technique, location accuracies of 1 wavelength and sizing accuracies of 2 wavelengths are attainable. It should be noted that the surface-spread function of all the sectioned flaws indicated that their surfaces acted as diffuse reflectors. Location and sizing accuracies associated with flaws that exhibit predominately specular behavior will probably differ from those defined in this discussion; but even in these cases, the accuracy will be very good, perhaps ±4 wavelengths.

The ability to obtain boundary locations based on analysis of the surface-spread function appears to be independent of amplitude for similiarly shaped flaws. For example, the boundaries of three separate horizontally oriented (relative to the scanned surface) cracks were determined within the defined accuracy even though the maximum amplitude associated with the cracks varied by 10 dB. All three cracks were located at comparable through-wall depths [2.7 to 2.9 inches (68 to 74 mm)] and were examined and processed using identical operating parameters. Variation in the maximum imaged amplitude was probably due to differences in the size and orientation of the reflective surface areas, which resulted in significant variations in the amount of reflected acoustic energy. Even with such variation in signal amplitude, the accuracy of flaw size measurements remained constant at ±2 wavelengths or better. These results, along with those from other tests, confirm the expectation that variations of signal amplitude will have little effect on the accuracy of sizing associated with SAFT UT.

*For the purpose of this report, surface-spread function describes a graphic representation of signal amplitude versus position at any defined plane. In the cases plotted, the planes were chosen to pass through image features requiring analysis. The shape of the graph then can be used for analysis of the flaw.

5. EXAMINATION RESULTS FROM THE BUTT-WELDED CARBON STEEL PLATE

During this project, a butt-welded carbon steel plate specimen was fabricated to contain four weld flaws. These included volumetric flaws such as porosity and slag inclusions and crack-type flaws in the form of weld metal cracking and heat-affected zone-to-base metal cracking. These four flaws (depicted in Figure 1) were examined using SAFT UT, radiography, and conventional manual UT. The manual UT examinations were performed using procedures defined by the ASME Boiler and Pressure Vessel Code, Section XI, 1974 Edition with Addenda through Summer 1975. However, Code requirements for manual UT were exceeded in that all indications down to 20 percent of the distance amplitude correction (DAC) curve were both recorded and plotted. Radiographs were performed using a 6 MeV LINAC Unit and a variety of orientations. After SAFT UT examinations were completed on all flaws, the specimen was destructively sectioned using locations defined by the SAFT UT image displays.

Both the sectioning and the results obtained from SAFT UT evaluation for each of the four flaws - porosity, slag inclusion, weld metal cracking, and heat-affected zone-to-base metal cracking - are presented in the following subsections in this section. For each flaw, two sets of SAFT UT color images are displayed. The first set is comprised of three images representing projections corresponding to the major (x, y, z) axes of the imaged volume. In each of these views, one axis is compressed so that the displayed amplitude of any pixel is the largest amplitude contained along the compressed axis. This type of display is useful in establishing the location, extent, and flaw shape along any axis.

The second set of SAFT UT color images represents planar slices through the flaw at locations and orientations corresponding to specific sections obtained during destructive examination. Photographs of the destructive sections are presented adjacent to the corresponding SAFT UT images so that they may be easily compared. The imaged-volume coordinates and axis labels shown on the SAFT UT image display are also annotated on the destructive sectioning photograph. Location and sizing estimates can be obtained by using the scales shown in each photograph and on the SAFT UT image displays. The major increment marks on all scales are 0.1 inch (2.54 mm) apart. It should be noted that in comparing SAFT UT images to the corresponding section photograph, two factors must be considered:

(1) The SAFT UT images define only those portions of the flaw that were acoustically reflective. The CRT images do not, for example, show the back side of porosity and slag inclusions.

(2) Section photographs show flaw regions as viewed at precisely defined planes while SAFT UT image displays are composed of pixels of finite dimensions 21 x 21 x 7 mils (0.53 x 0.53 x 0.18 mm) and exhibit a resolution dependent upon the wavelength of the ultrasonic frequency used for the inspection. It is possible, therefore, for SAFT UT images to show more or larger flaws than are shown in section photographs.

Sizing predictions using surface-spread functions for selected data also are discussed and presented in graphs for each of the four flaws. Where practical, measurements were made on the actual flaw surface regions

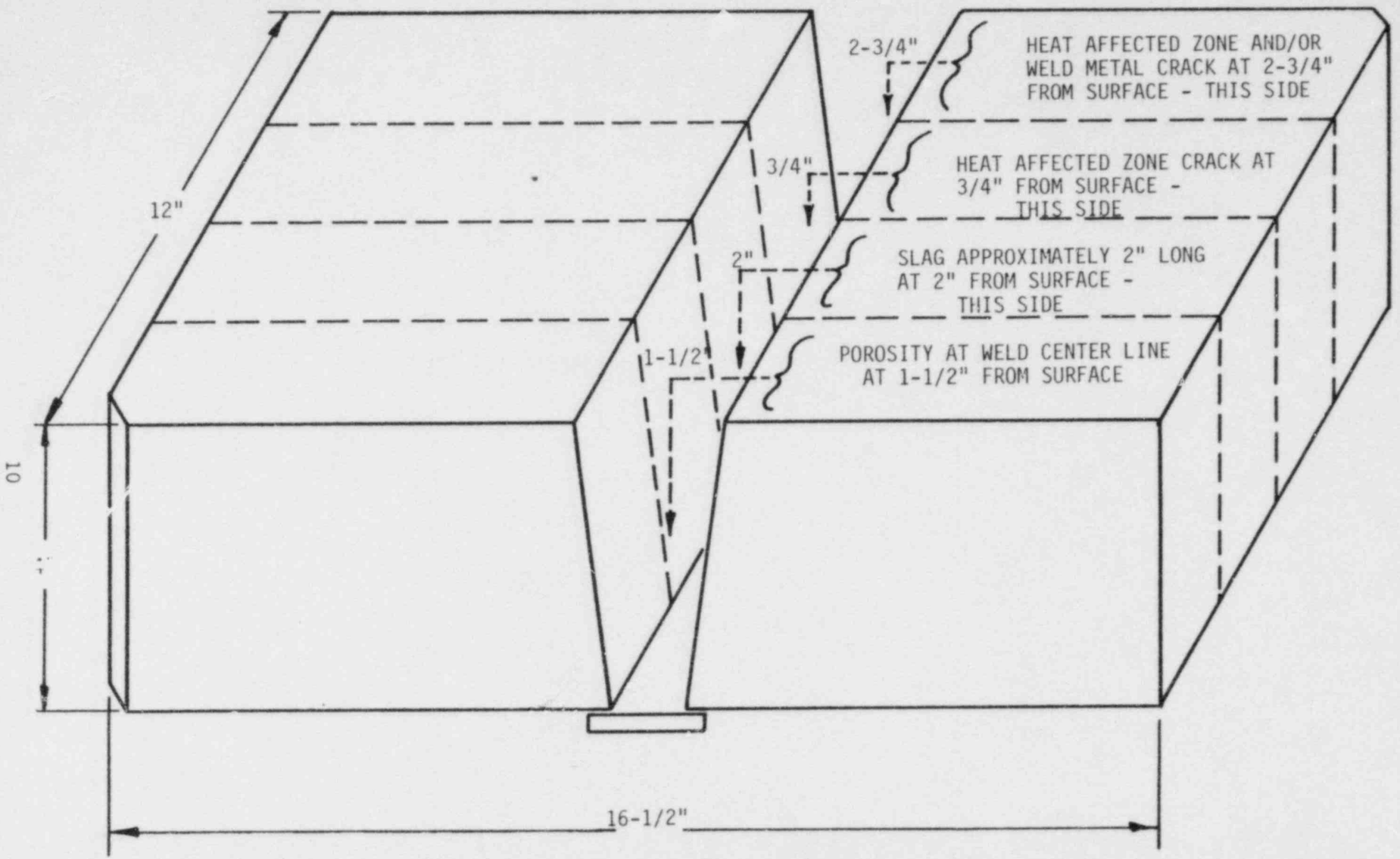

FIGURE 1. BUTT-WELDED CARBON STEEL PLATE SPECIMEN - POROSITY

corresponding to the surface-spread function data. In some cases, these measurements involved visually estimating what portion of the flaw surface was acoustically reflective. In all cases, the size measurement shown in the plotted data figures represents the visually determined size with an accuracy of ±0.025 inch (0.63 mm). Where measurements were not possible, no value is shown.

5.1 Porosity Region

The imaged porosity region contained within the butt-welded carbon steel plate is shown in Figures 2, 3, and 4. These three figures are compressed CRT presentations and, therefore, show a composite of the acoustically reflective surfaces viewed from the corresponding axis projection. Information defining the location, size, and shape relative to the entire reconstructed volume can be obtained from these views.

5.1.1 Destructive Sectioning

Destructive sectioning was performed by sawing the specimen at locations defined by study of SAFT UT images. Two views of this sectioning are shown in Figures 6 and 9, which represent B-scan- and C-scan-type viewing orientations of the flaw.

The C-scan-type presentations are shown in the CRT color image in Figure 5 and its corresponding cross-section photograph in Figure 6. The spaces between the sectioned pieces represent the approximate amount of material lost during the cutting and grinding activities. The saw cut made to reveal this porosity region exposed numerous separate pits of varying sizes and shapes. The SAFT UT image shows the acoustically reflective surfaces of these pits. These surfaces were destroyed by the saw cut [approximately 0.07 inch (1.7 mm) thick] and only the voids existing below the reflecting surfaces remain. This flaw also was composed of numerous discrete reflectors which, in many cases, were smaller than 1 wavelength and separated from adjacent flaws by less than 1 wavelength. The SAFT UT image shows numerous separate reflectors at locations that correlate well with the pit locations shown in the section photographs.

The B-scan presentations of the section are shown in Figures 8 and 9. Again, the reflecting surfaces consist of numerous separate pits of varying sizes and shapes. These characteristics are also shown in the SAFT UT image using a 8 dB down threshold.

Lateral sizing predictions for one of the discrete reflectors are shown in Figure 7 using the surface-spread function at selected image locations. Although the reflective surfaces were destroyed during sectioning, these lengths appear reasonable (within 1 wavelength) based on the size of the exposed pits. Flaw z-axis through-wall locations determined by analysis of the depth-spread function also indicate at least 1 wavelength resolution using 8 dB down threshold.

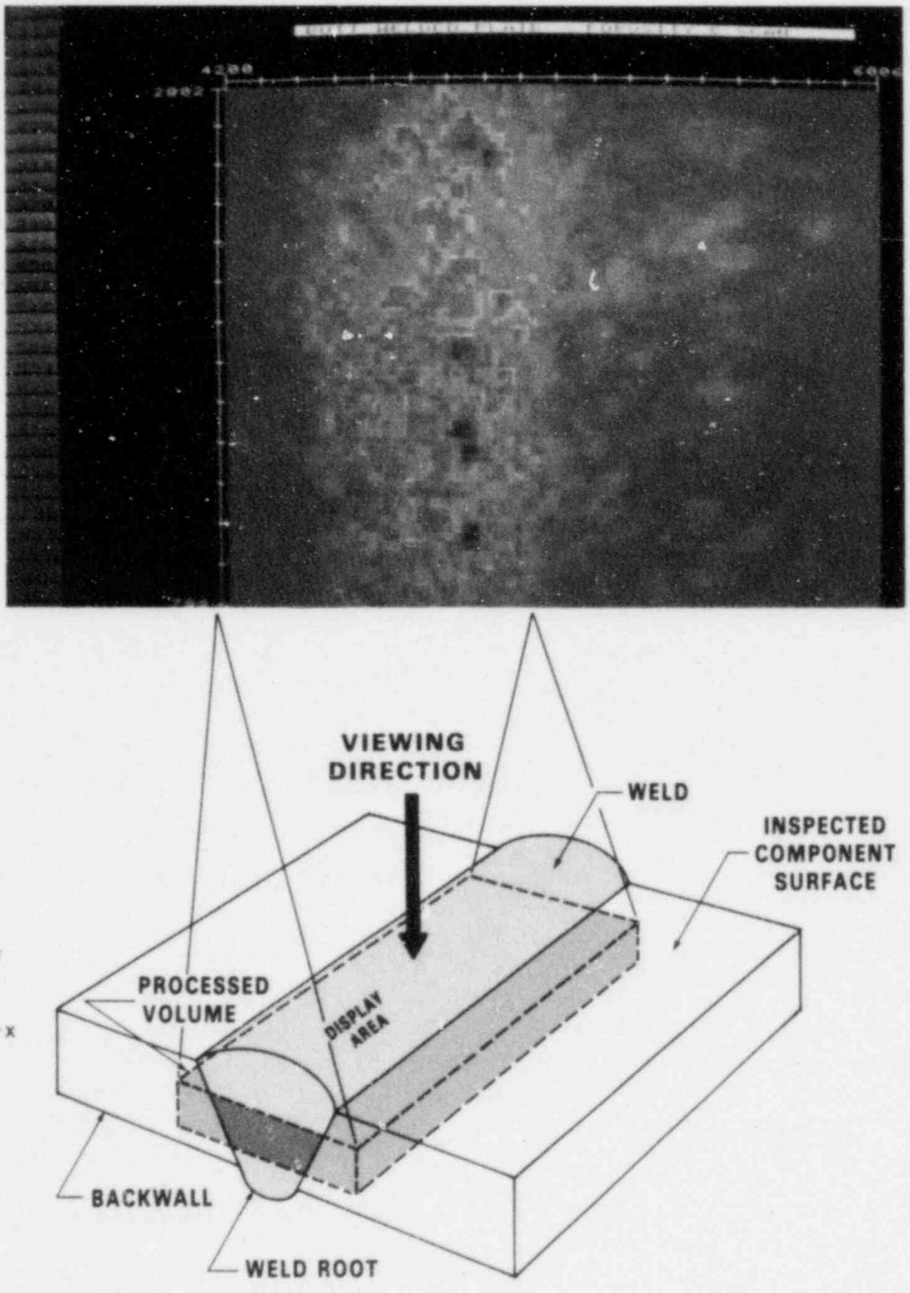

FIGURE 2. BUTT-WELDED CARBON STEEL PLATE SPECIMEN - POROSITY
(C-Scan View)

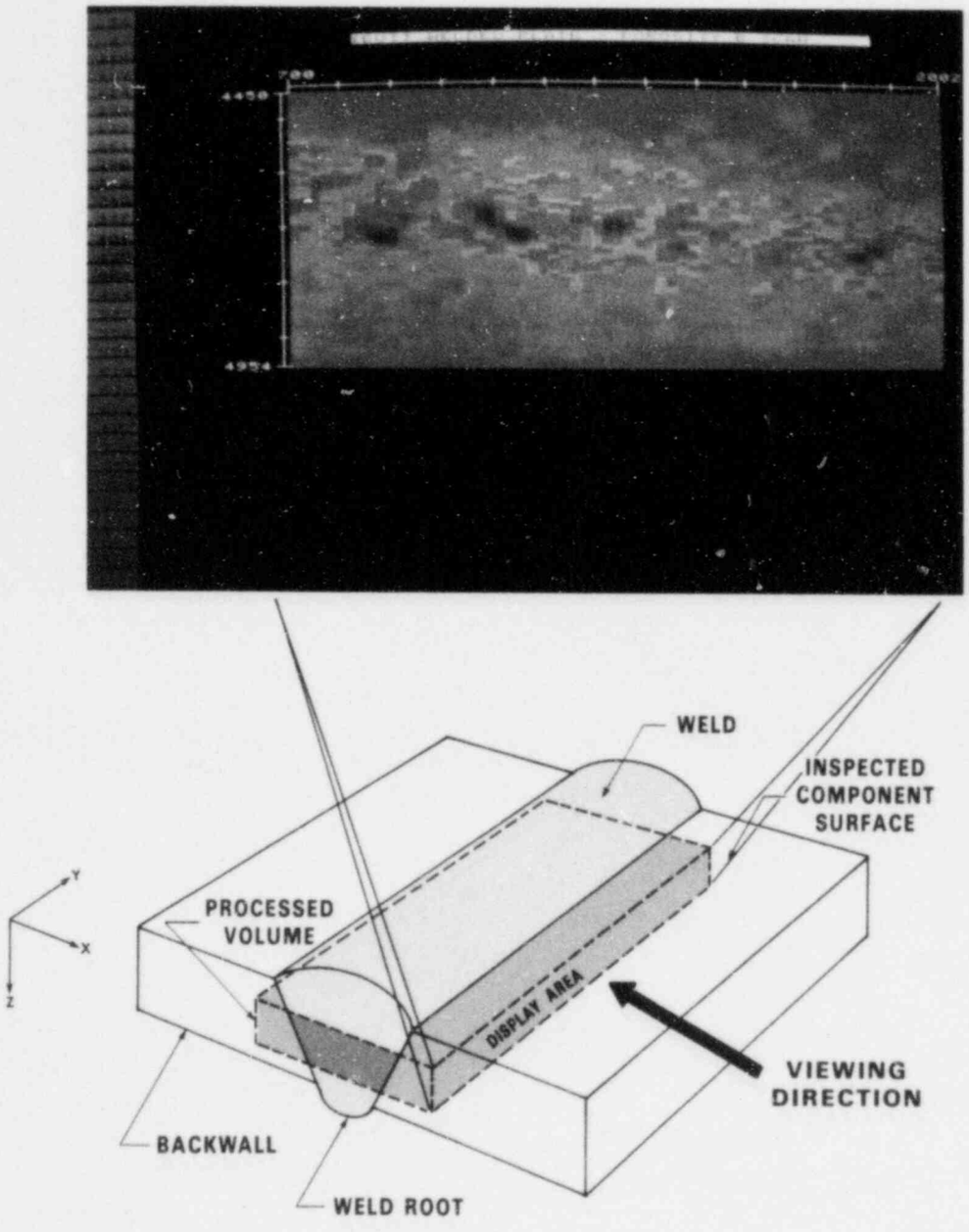

FIGURE 3. BUTT-WELDED CARBON STEEL PLATE SPECIMEN - POROSITY
(B-Scan View Parallel to Weld)

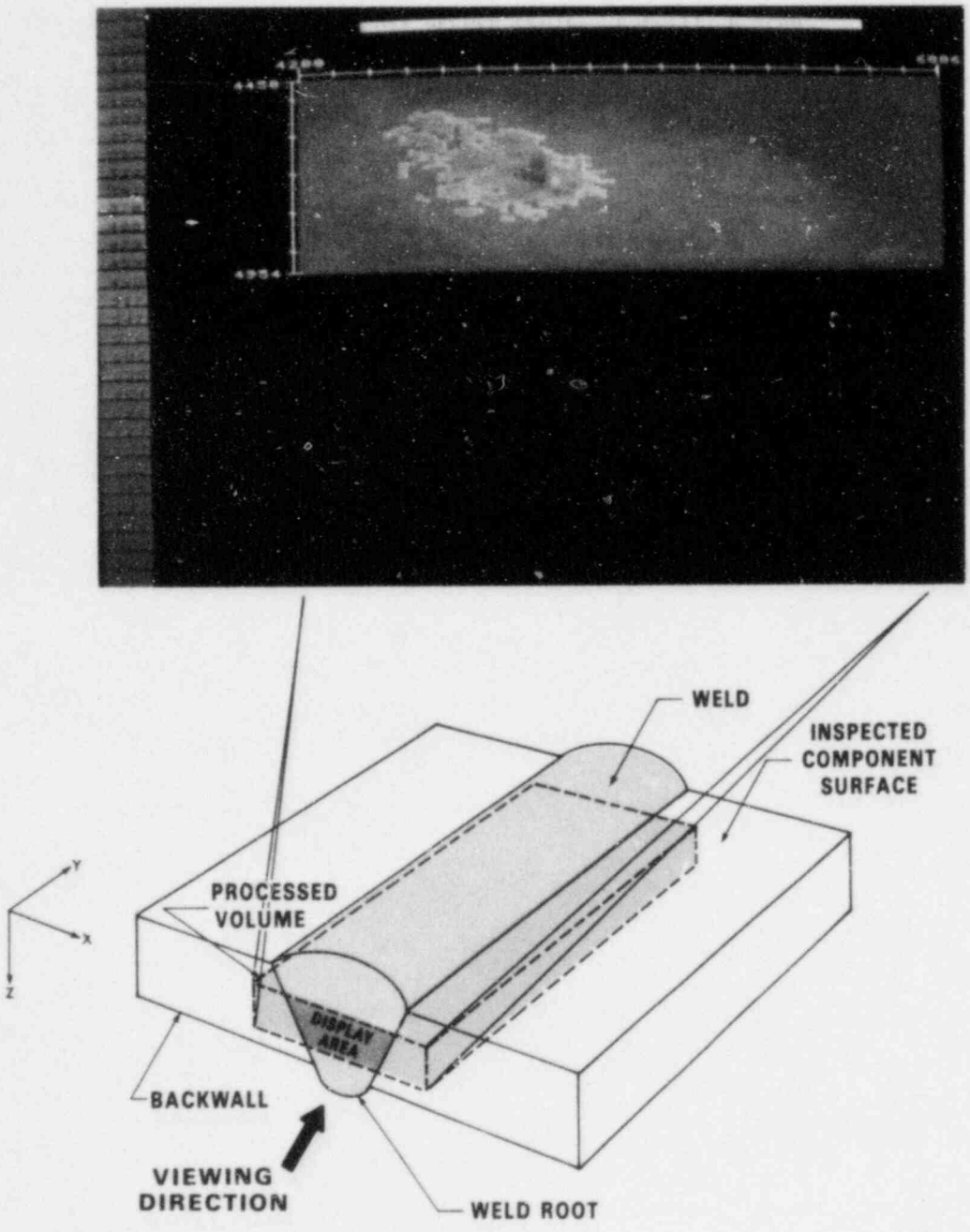

FIGURE 4. BUTT-WELDED CARBON STEEL PLATE SPECIMEN - POROSITY
(B-Scan View Transverse to Weld)

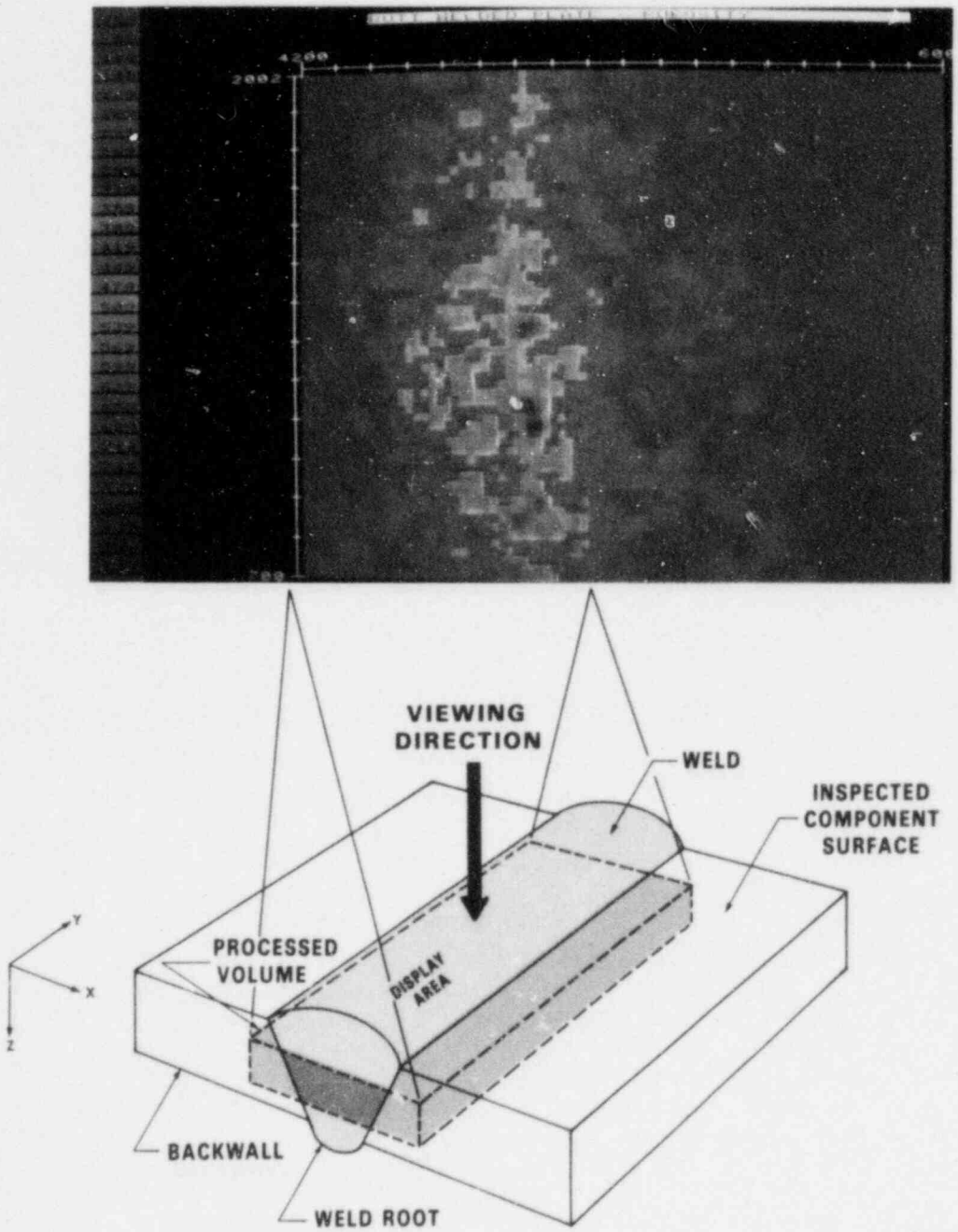

FIGURE 5. BUTT-WELDED CARBON STEEL PLATE SPECIMEN - POROSITY SECTION
(C-Scan View)

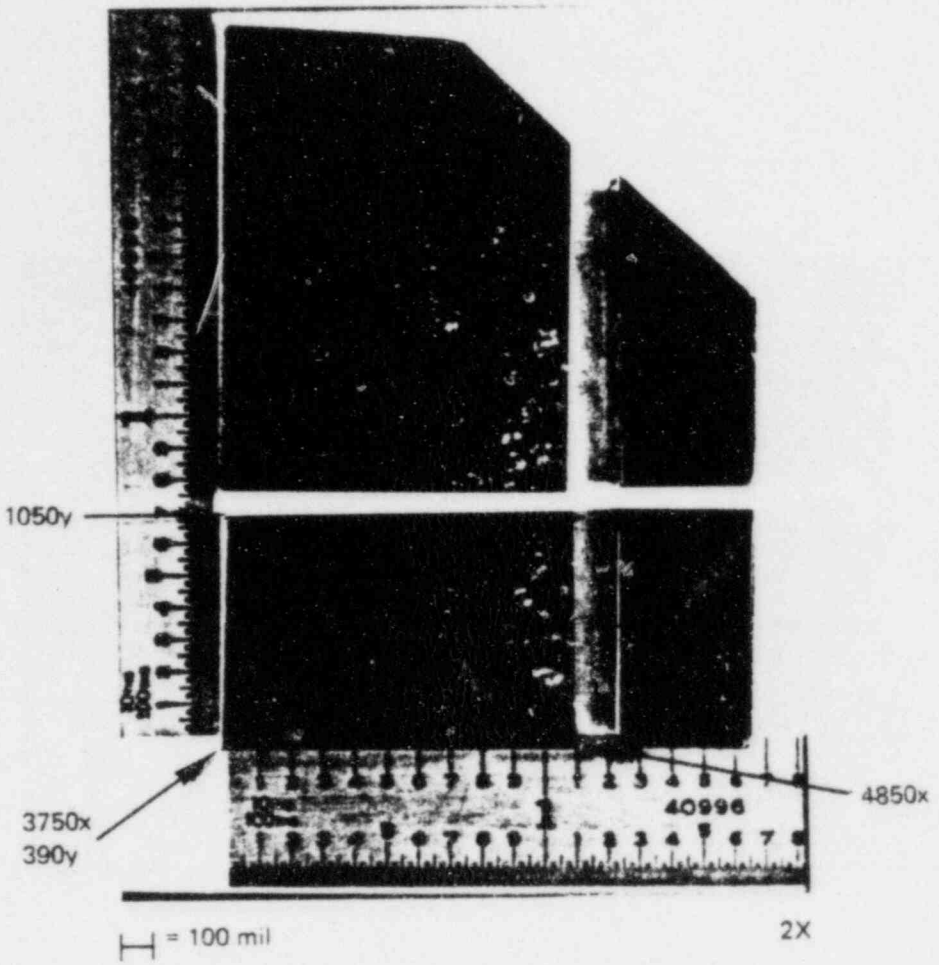

FIGURE 6. BUTT-WELDED CARBON STEEL PLATE - POROSITY REGION
(C-scan section at z=4660)

Sectioned specimen pieces are shown with the approximate amount of material destroyed during sawing and grinding indicated by the spaces between the pieces. Coordinate and axis labels corresponding to the imaged volume are annotated. Note that the imaged volume y-axis lower limit begins 300 mils from the lower edge of the sectioned specimen. Through-wall depth of this plane is ≈1450 mils (0.935 mm).

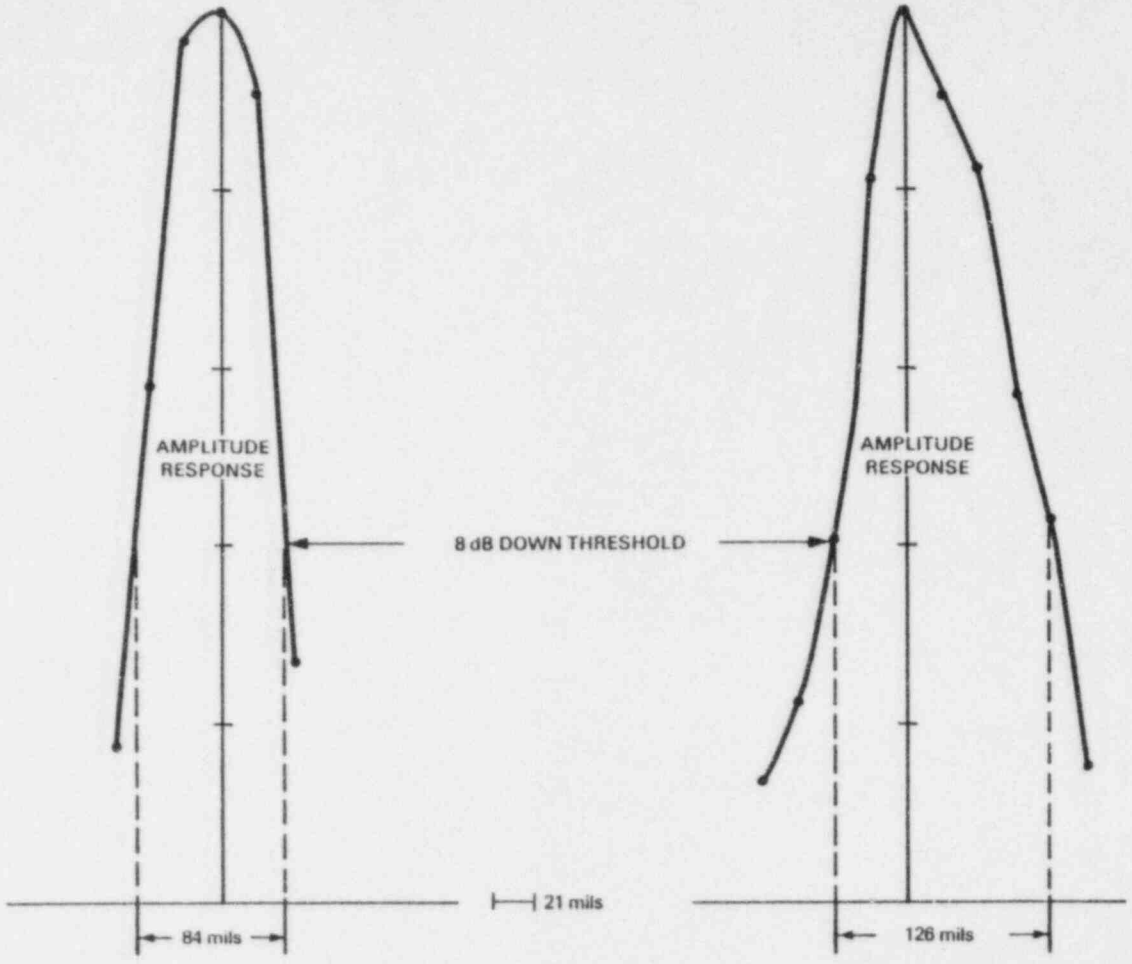

Lateral Distance

(a) X-Axis Length Using Data at X = 4820, Z = 4700

Lateral Distance

(b) X-Axis Length Using Data at Y = 1320, Z = 4700

FIGURE 7. SIZE PREDICTIONS USING THE SURFACE-SPREAD FUNCTION: BUTT-WELDED CARBON STEEL PLATE - POROSITY REGION (X- and Y-Axis Lengths for a Pit Centered at the 4820, 1320, and 4700 Coordinates in the Imaged Volume Display)

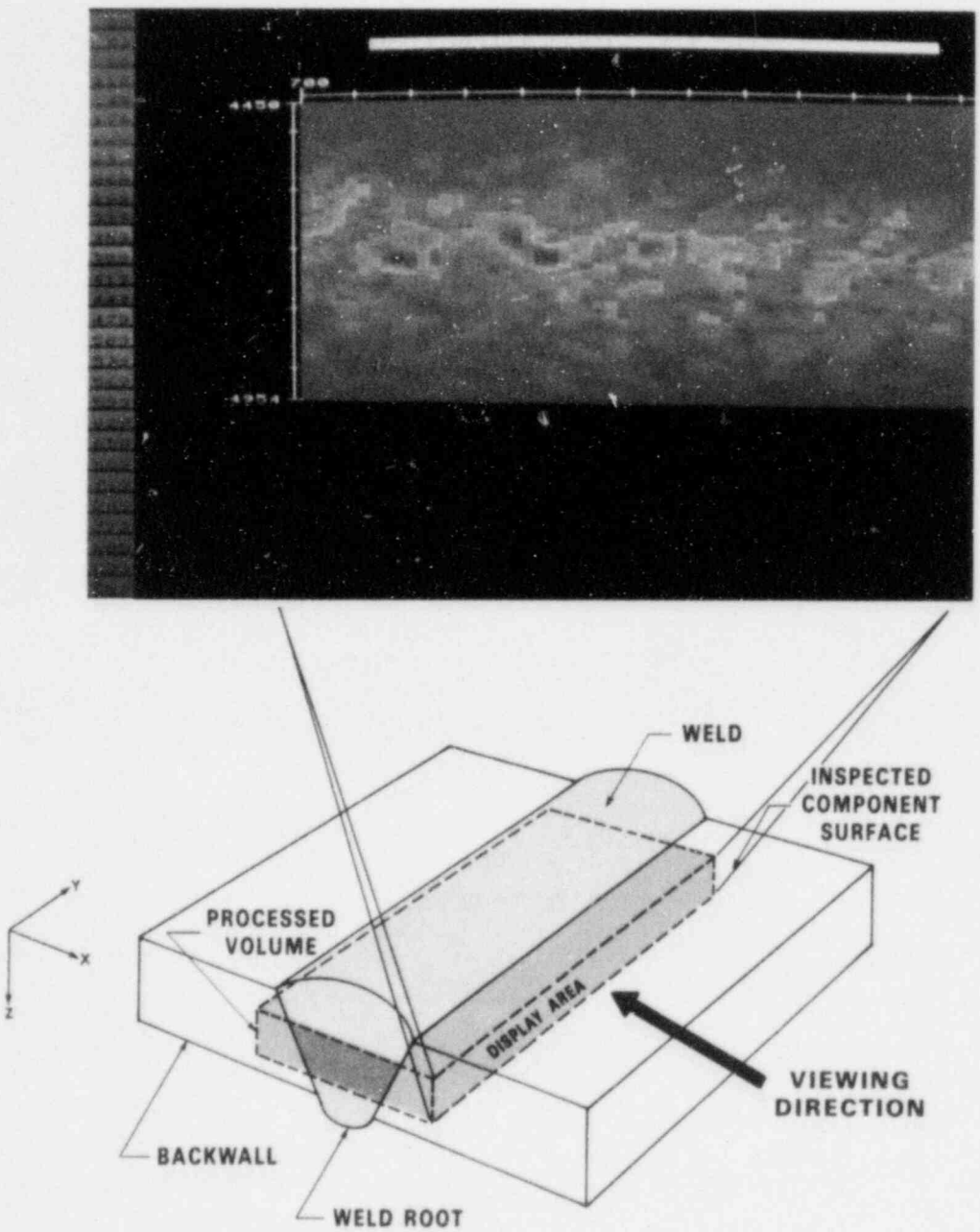

FIGURE 8. BUTT-WELDED CARBON STEEL PLATE SPECIMEN - POROSITY SECTION
(B-Scan View Parallel to Weld)

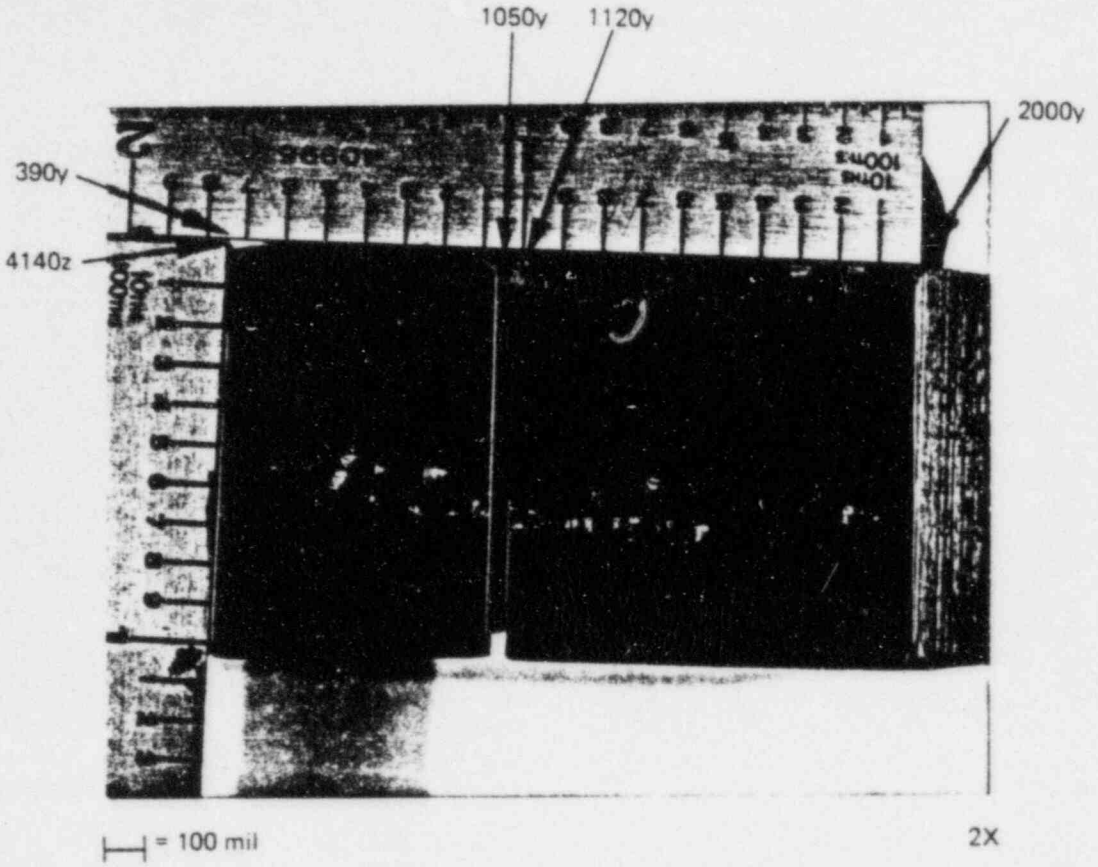

FIGURE 9. BUTT-WELDED CARBON STEEL PLATE - POROSITY REGION
(B-scan section at x=4850)

Sectioned specimen pieces are shown with the approximate amount of material destroyed during sawing and grinding indicated by the spaces between the pieces. Coordinate and axis labels corresponding to the imaged volume are annotated. Note that the imaged volume y-axis lower limit begins 300 mils from the left side of the sectioned specimen. Through-wall depths can be determined by subtracting the front surface location [3210 mils (81.5 mm)] from any z-axis location.

5.1.2 Radiography

Radiographic examination of this porosity flaw produced results very similar to the SAFT UT image shown in Figure 2. Small discrete pits could be seen at the periphery of the flaw region with a large continuous discontinuity visible throughout the major area of the flaw.

5.1.3 Manual UT Examination Results

No recordable indications (20 percent DAC or above) were noted in this flaw region using 0-, 45- or 60-degree inspection angles.

5.2 Slag Inclusion Region

The imaged slag inclusion region contained within the butt-welded carbon steel plate is shown in Figures 10, 11 and 12. These three figures are compressed view presentations and, therefore, show a composit of the flaw viewed from the corresponding axis projection. Information defining the location, size, and shape relative to the entire imaged volume can be obtained from these views.

5.2.1 Destructive Sectioning

Destructive sectioning was performed by sawing the specimen at locations defined by studying the SAFT UT images. Two views of this section are shown in Figures 14 and 16 that represent B-scan- and C-scan-type viewing orientations of the flaw.

The B-scan-type presentation is shown in Figures 13 and 14. At this location, the inclusion has a shape similar to the letter "L." The corresponding SAFT UT image shows those flaw surface features that were favorably oriented to the ultrasound and were, therefore, acoustically reflective. In this case, the right and left sides of the vertical leg of the "L" were not imaged, but the top surfaces (approximately horizontal) of the vertical and horizontal legs of the "L" were imaged and show up clearly. This provides clear evidence that vertically oriented flaw surfaces are difficult to image using a 0-degree inspection mode because of the very low acoustic reflectivity characteristics at this angle.

The C-scan-type presentations are shown in Figures 15 and 16. The sectioning cut was made so that the reflecting surface corresponding to the top of the "L" was preserved. A rubber replica was made of this portion of the flaw surface so that it could be studied in detail. The replica facilitated measurement of surface angles relative to the direction of the insonifying ultrasound. Analysis showed that those surface features favorably oriented to the acoustic energy were clearly imaged and resolvable, and those moderately or highly angulated to the direction of the incoming ultrasound were not imaged. Sizing predictions for selected x-axis lengths are shown for four separate locations in Figure 17. Also annotated on Figure 17 are the sizes determined by measuring that portion of the flaw surface estimated to be acoustically reflective for the 0-degree examination direction. Three of these lengths (a through c) represent surface-spread functions for different parts of the top of the vertical leg of the "L."

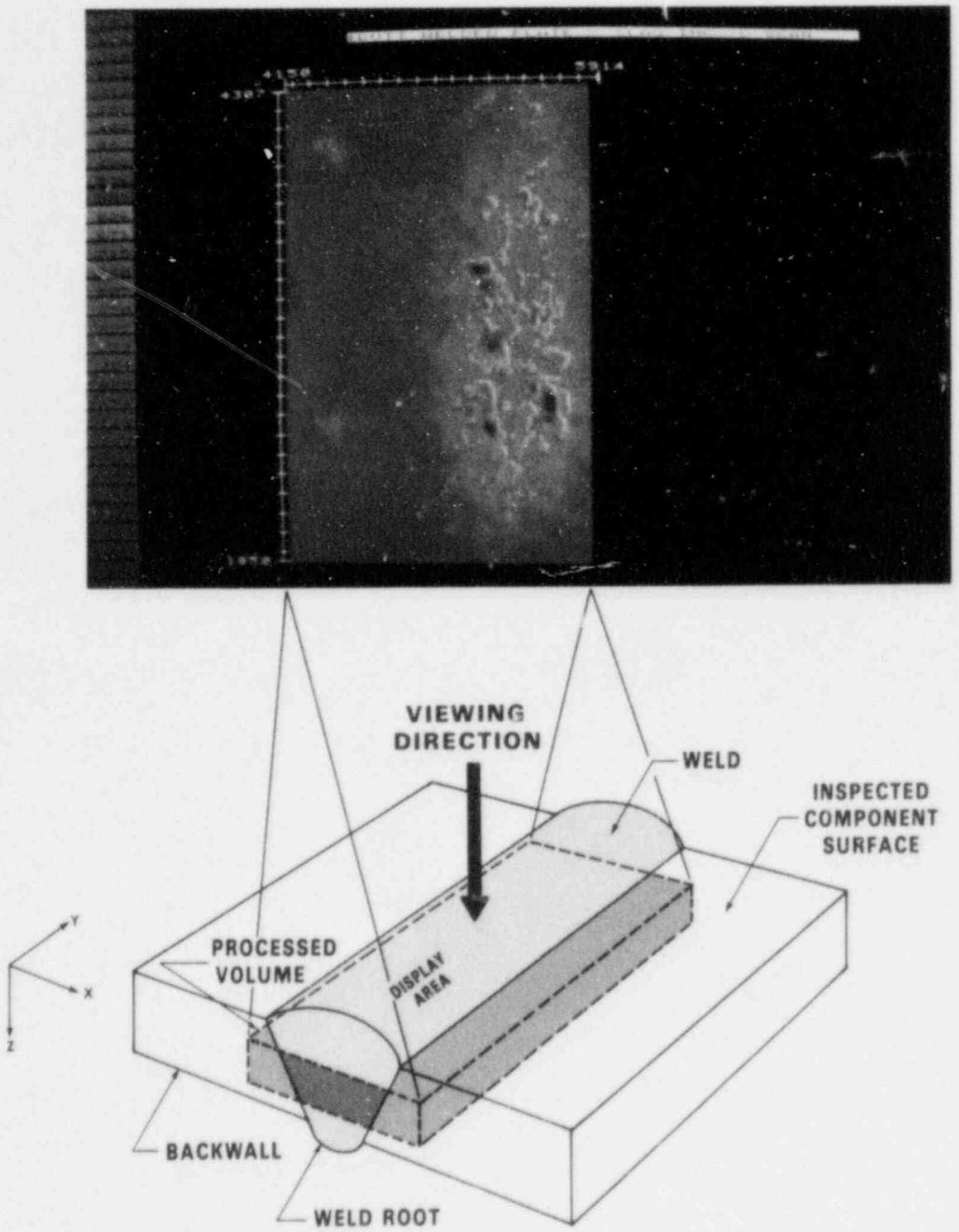

FIGURE 10. BUTT-WELDED CARBON STEEL PLATE SPECIMEN - SLAG INCLUSION
(C-Scan View)

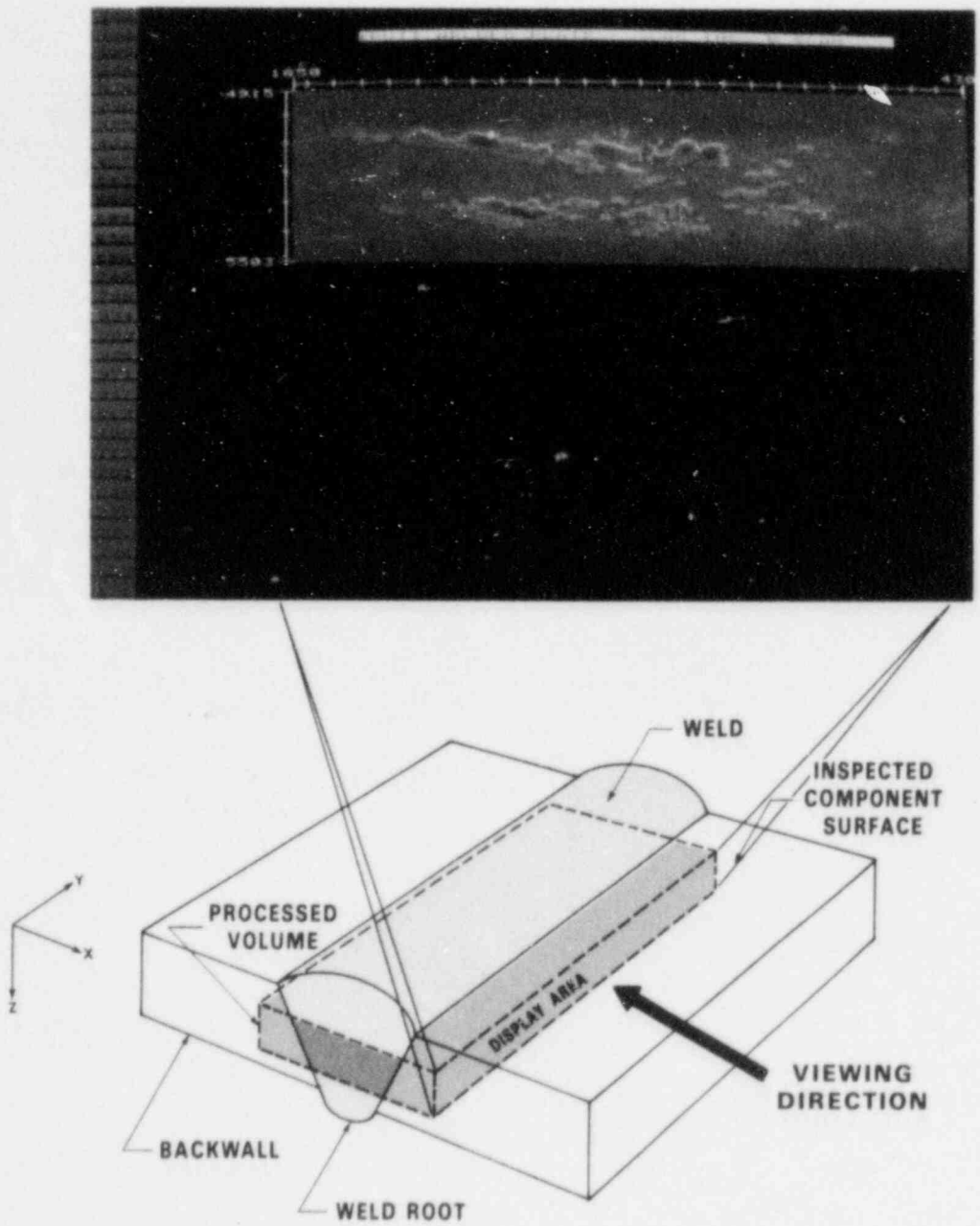

FIGURE 11. BUTT-WELDED CARBON STEEL PLATE SPECIMEN - SLAG INCLUSION
(B-Scan View Parallel to Weld)

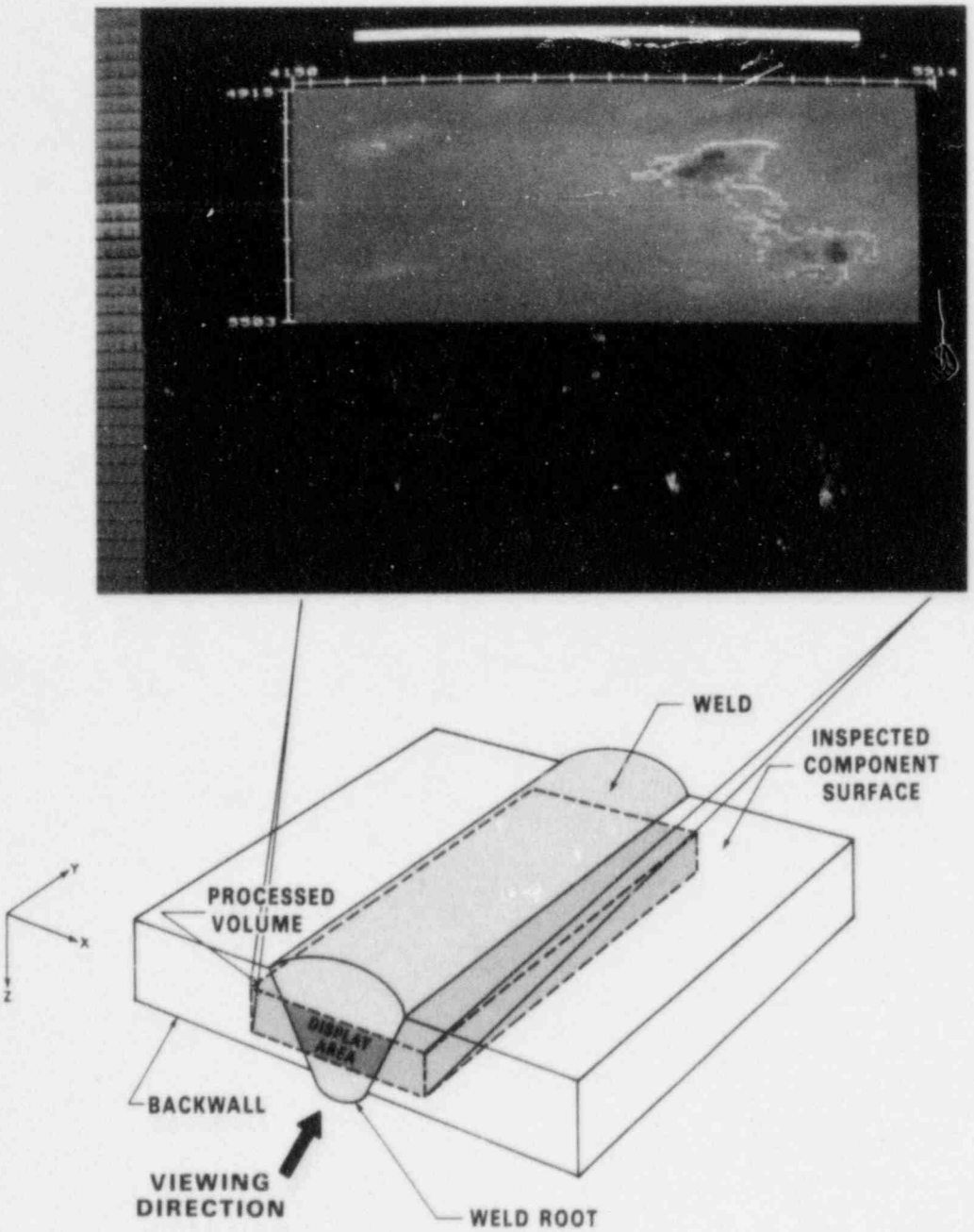

FIGURE 12. BUTT-WELDED CARBON STEEL PLATE SPECIMEN - SLAG INCLUSION
(B-Scan View Transverse to Weld)

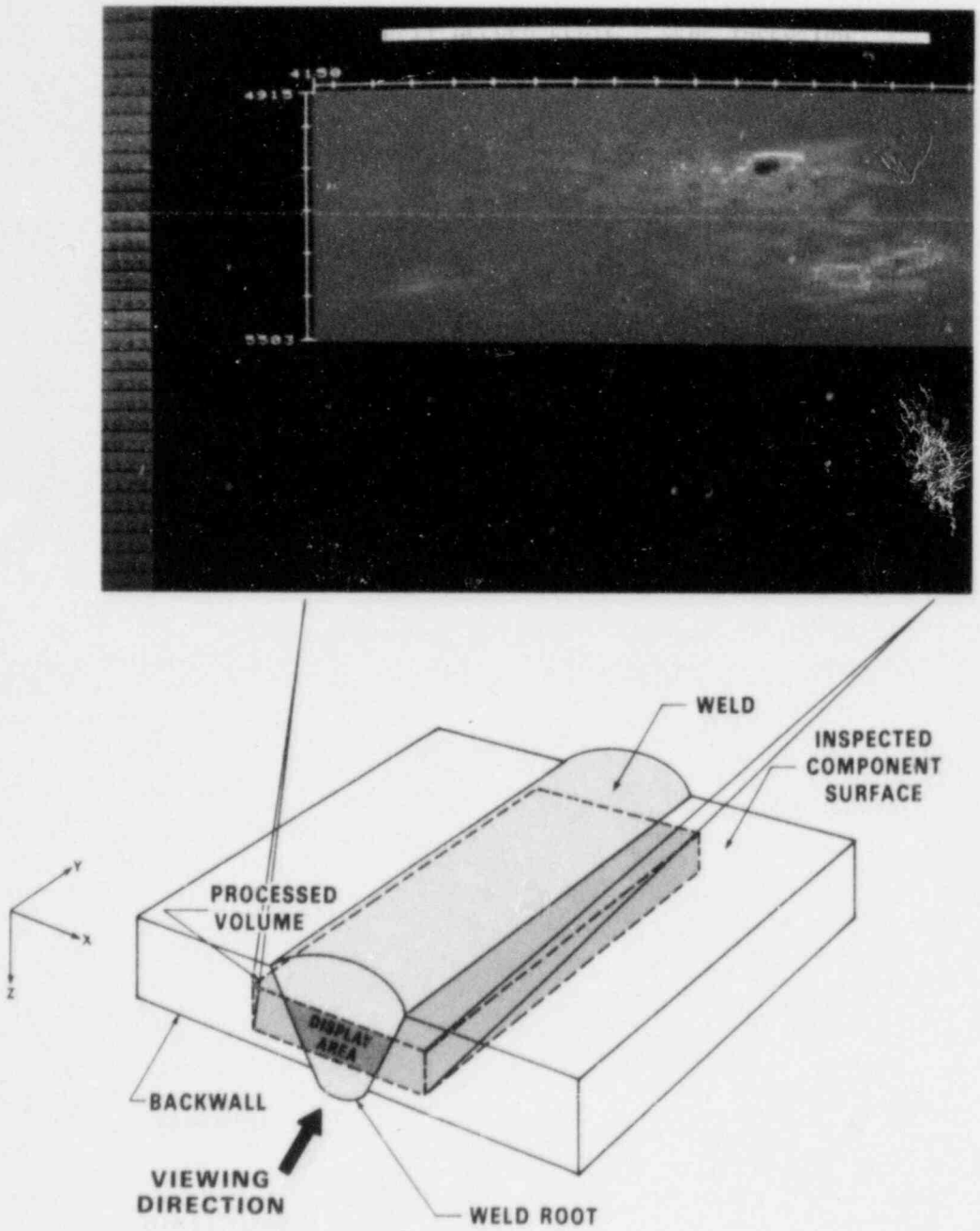

FIGURE 13. BUTT-WELDED CARBON STEEL PLATE SPECIMEN - SLAG INCLUSION SECTION
(B-Scan View Transverse to Weld)

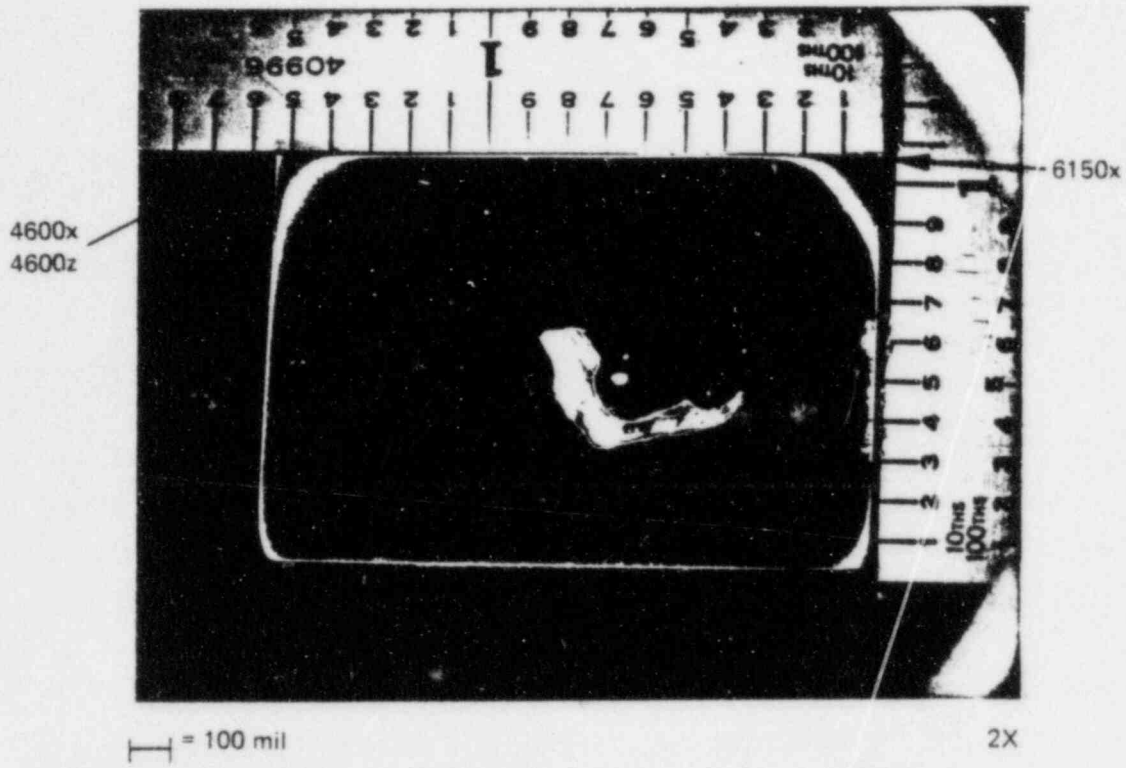

FIGURE 14. BUTT-WELDED CARBON STEEL PLATE - SLAG INCLUSION REGION (B-scan section at y≈2450)

Sectioned specimen piece shown with coordinate and axis labels corresponding to the imaged volume. Through-wall depths can be determined by subtracting the front surface location [3170 mils (80.5 mm)] from any z-axis location.

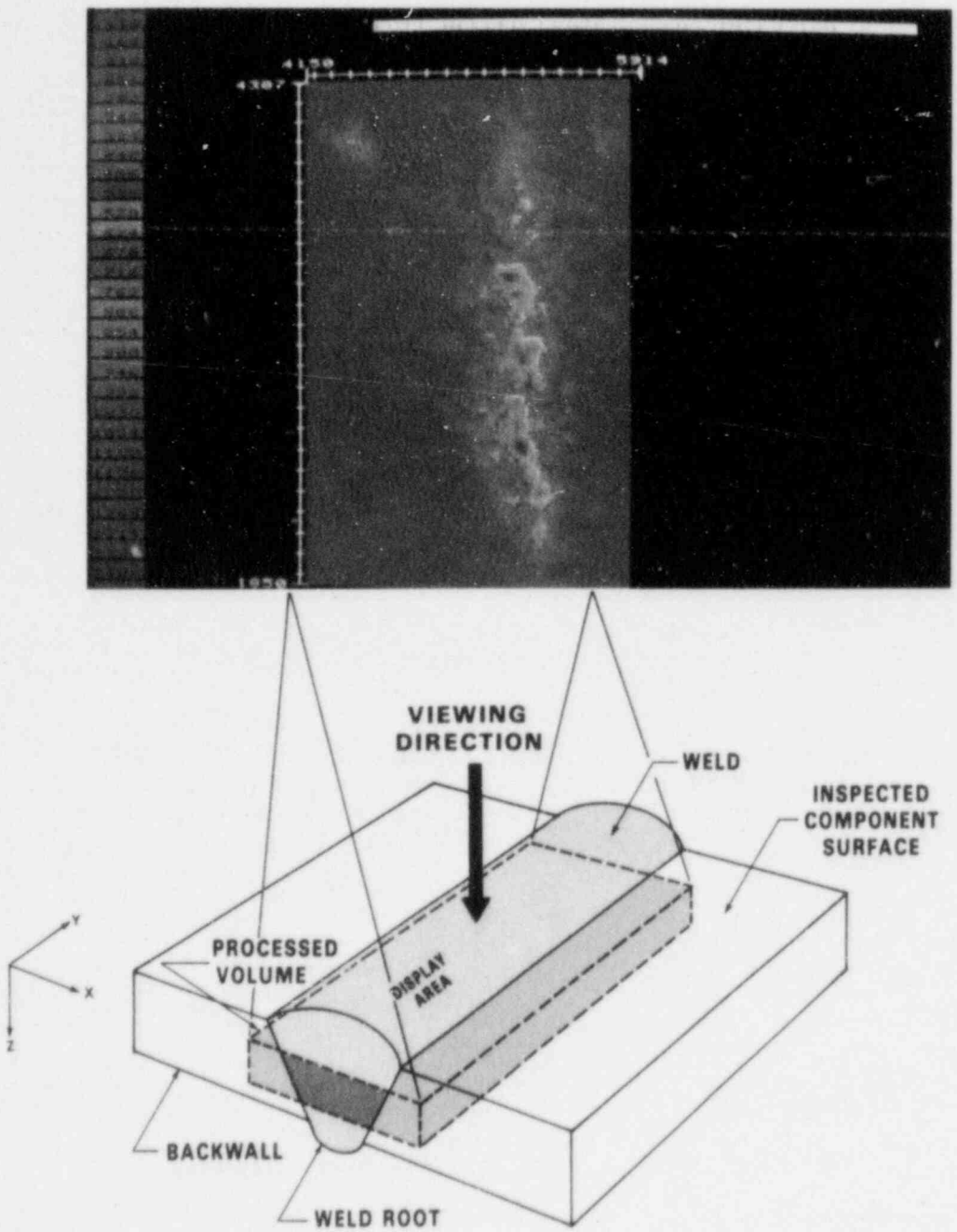

FIGURE 15. BUTT-WELDED CARBON STEEL PLATE SPECIMEN - SLAG INCLUSION SECTION (C-Scan View)

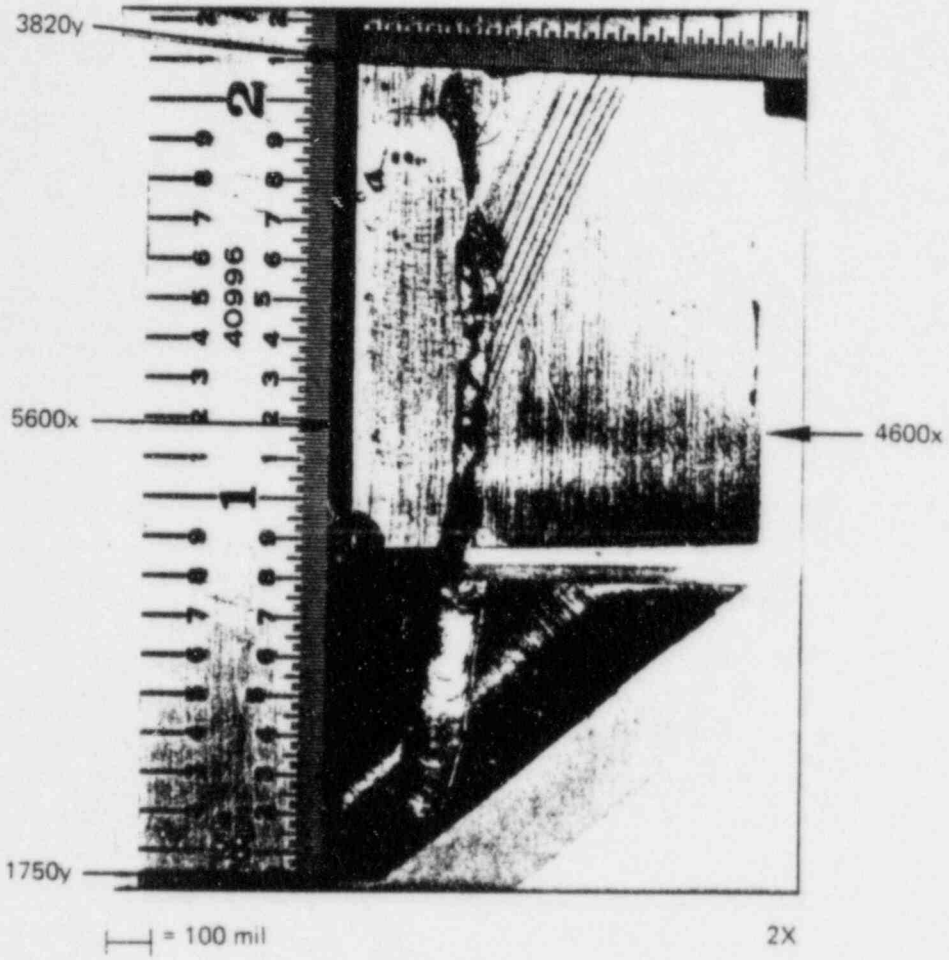

FIGURE 16. BUTT-WELDED CARBON STEEL PLATE - SLAG INCLUSION REGION (C-scan section at z≈5150)

Sectioned specimen pieces are shown with the approximate amount of material destroyed during sawing and grinding indicated by the space between the pieces. Coordinate and axis labels corresponding to the imaged volume are annotated. Note that the x-axis location values increase from right to left instead of left to right as presented in the SAFT UT image. This is caused by viewing the reflective surface of the flaw from a direction opposite of that used in the SAFT UT image display. Through-wall depth of this plane is ≈1980 mils (50.3 mm).

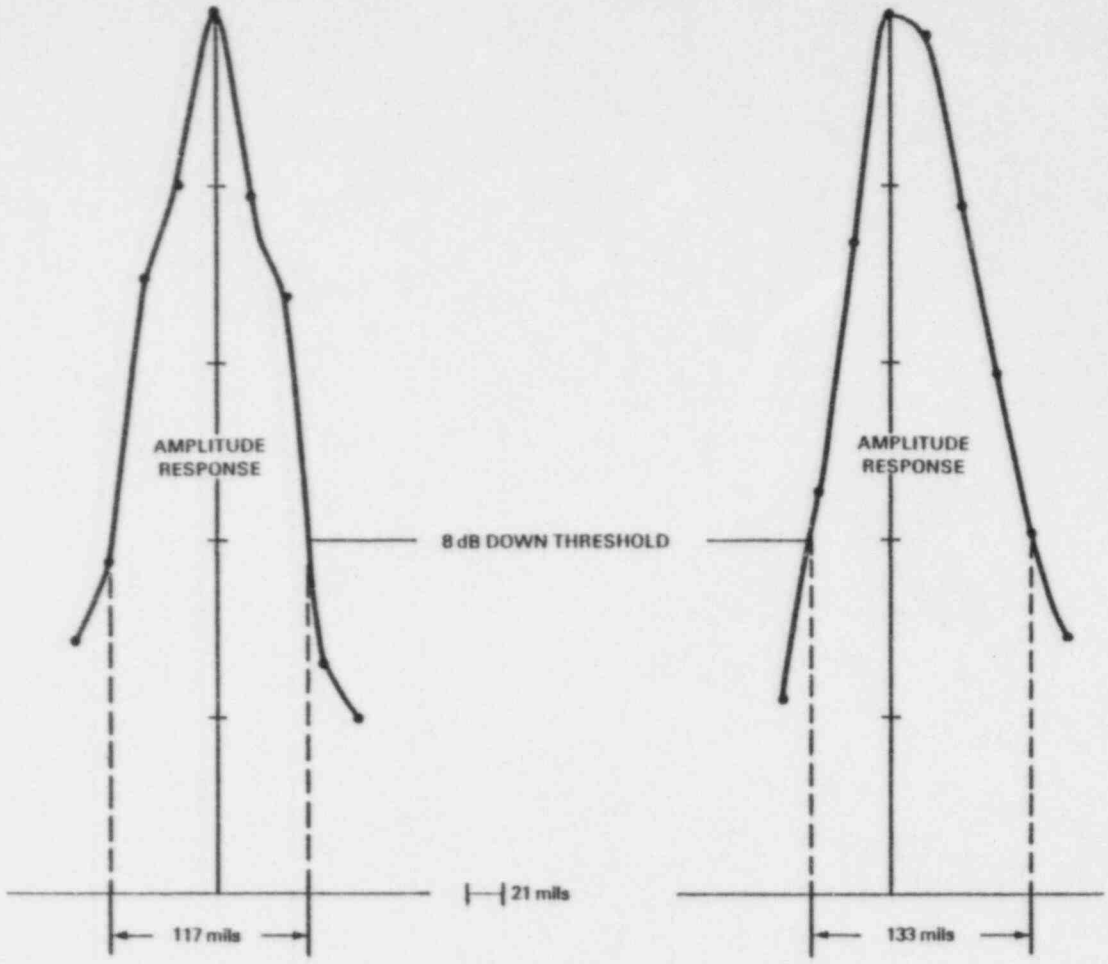

(a) X-Axis Length Using Data at Y = 2100, Z = 5080, Measured Size = 45 mils

(b) X-Axis Length Using Data at Y = 2520, Z = 5095, Measured Size = 80 mils

FIGURE 17. SIZE PREDICTIONS USING THE SURFACE-SPREAD FUNCTION: BUTT-WELDED CARBON STEEL PLATE - SLAG INCLUSION REGION (X-Axis Lengths for Top of Vertical Leg Features of 'L' Shaped Defect)

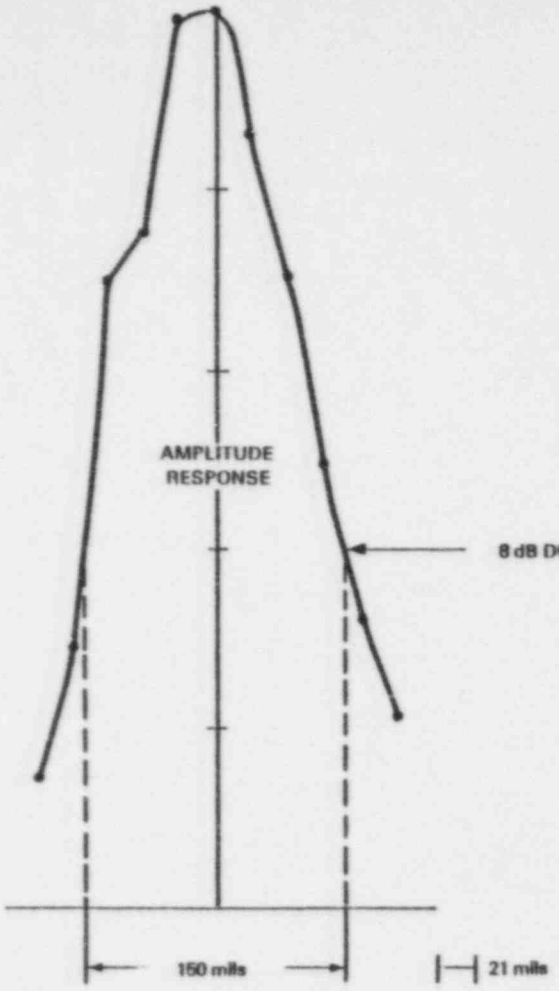

(c) X-Axis Length Using Data at Y = 3325, Z = 5130, Measured Size = 105 mils

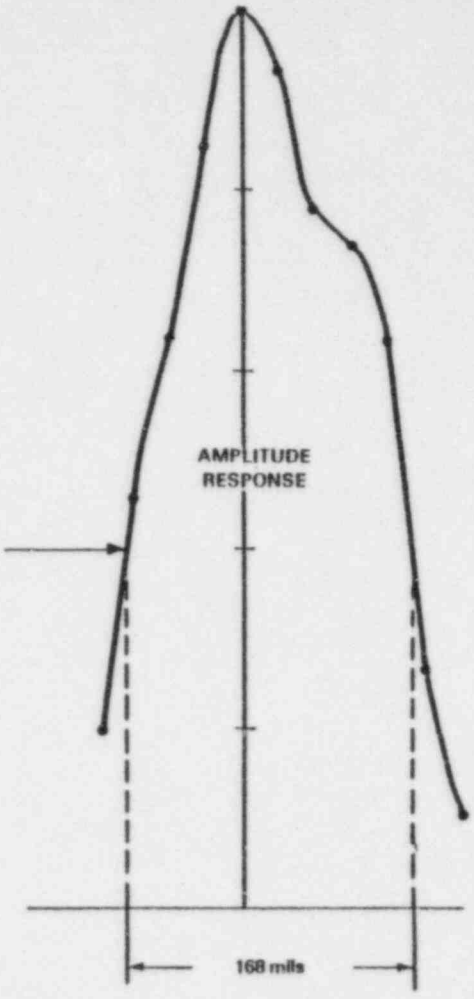

(d) X-Axis Length Using Data at Y = 2450, Z = 5335, Measured Size = 105 mils

FIGURE 17 (Cont'd). SIZE PREDICTIONS USING THE SURFACE-SPREAD FUNCTION: BUTT-WELDED CARBON STEEL PLATE - SLAG INCLUSION REGION (X-Axis Lengths for Top of Vertical and Horizontal Leg Features of 'L' Shaped Defect)

The fourth surface-spread function, d, represents the x-axis length for part of the horizontal leg of the "L" centered at x = 5450. Evaluation of z-axis through-wall locations using the depth-spread function at selected locations demonstrates a resolution capability of at least 1 wavelength using an 8 dB down threshold.

5.2.2 Radiography

Radiographic examination of this flaw produced results very similar to the SAFT UT image shown in Figure 10 with the exception that flaw features corresponding to the lower 0.03 inch (7.6 mm) of the flaw are better defined. The large slag-filled voids provided significant discontinuities in the material density and resulted in radiographic photographs in which the slag inclusion region is well defined (C-scan-type viewing orientation).

5.2.3 Manual UT Examination Results

A manual UT examination was performed by a certified Level II examiner using procedures defined in Section XI of the ASME Code. Sizing estimates were performed by a certified Level III examiner using only the information recorded on the Calibration Record and Examination Record data sheets. Table 1 represents a summary of the location and sizing information for manual UT, SAFT UT, and destructive examination measurements. All coordinates shown are relative to the imaged volume used in the SAFT UT inspection. For the manual inspection, three reflectors were established by the Level III analysis; therefore, three entries are made in each category in the table. The results shown in Table 1 reflect the maximum defect extent for the indicated measurement or location.

The SAFT UT images indicate that this flaw is composed of numerous reflective surfaces in close proximity to each other. The size reported in Table 1 for SAFT UT represents the collective size of all reflecting surfaces which are within four wavelengths of any neighboring surface.

5.3 Weld-Metal Cracking and Porosity Region

The imaged weld-metal cracking region contained within the butt-welded carbon steel plate is shown in Figures 18, 19, and 20. These three figures are compressed view presentations and, therefore, show a composite of the acoustically reflective surfaces viewed from the corresponding axis projection. Information defining the location, size, and shape relative to the entire imaged volume can be obtained from these views.

5.3.1 Destructive Sectioning

Destructive sectioning was performed by sawing the specimen at locations defined by the SAFT UT image displays. Three sections are shown which represent B-scan-type viewing orientations of these flaws. By design, this region was supposed to contain an example of heat-affected-zone cracking. However, destructive sectioning revealed that all the flaws existing within this imaged volume were located entirely within the weld metal. B-scan (transverse to weld) presentations of the SAFT UT image and the corresponding sectioned specimen photograph are shown in Figures 21 and 22; these reveal the presence of a small 0.07-inch (1.7-mm) horizontally oriented crack.

TABLE 1. SUMMARY OF THE LOCATION AND SIZING INFORMATION FOR SLAG INCLUSION USING MANUAL UT, SAFT UT, AND DESTRUCTIVE EXAMINATION MEASUREMENTS

	EXAMINATION METHOD		
	Manual UT (Three Reflectors Defined by Nine Recorded Indications)	SAFT UT (Using an 8 dB Down Threshold on the Surface-Spread Function)	Destructive Examination (Maximum Flaw Length)
SIZE (Measured in inches)			
Length - max. length parallel to weld	a. 0.75 b. 1.43 c. 4.0	1.75	1.97
Width - max. length transverse to weld	Unavailable - W_{max} only recorded	0.67	0.58
Depth - max. length in through-wall	a. 0.0625 - 0.125 b. 0.125 - 0.1875 c. 0.0625 - 0.250 (Based on amplitude only)	0.35	0.32
LOCATION (Imaged coordinate locations measured in mils - accuracy ±100 mils)			
Length - lower and upper limits parallel to weld	a. 3320 - 4070 b. 1890 - 3320 c. 700 - 4700	2050 - 3800	1850 - 3820
Width - lower and upper limits transverse to weld	a. 4600 b. 4900 c. 5270 (Based on W_{max} only)	5070 - 5740	5200 - 5780
Depth - lower and upper limits in through-wall	a. 5370 b. 5370 c. 5270 (Based on W_{max} only)	5050 - 5400	5030 - 5350

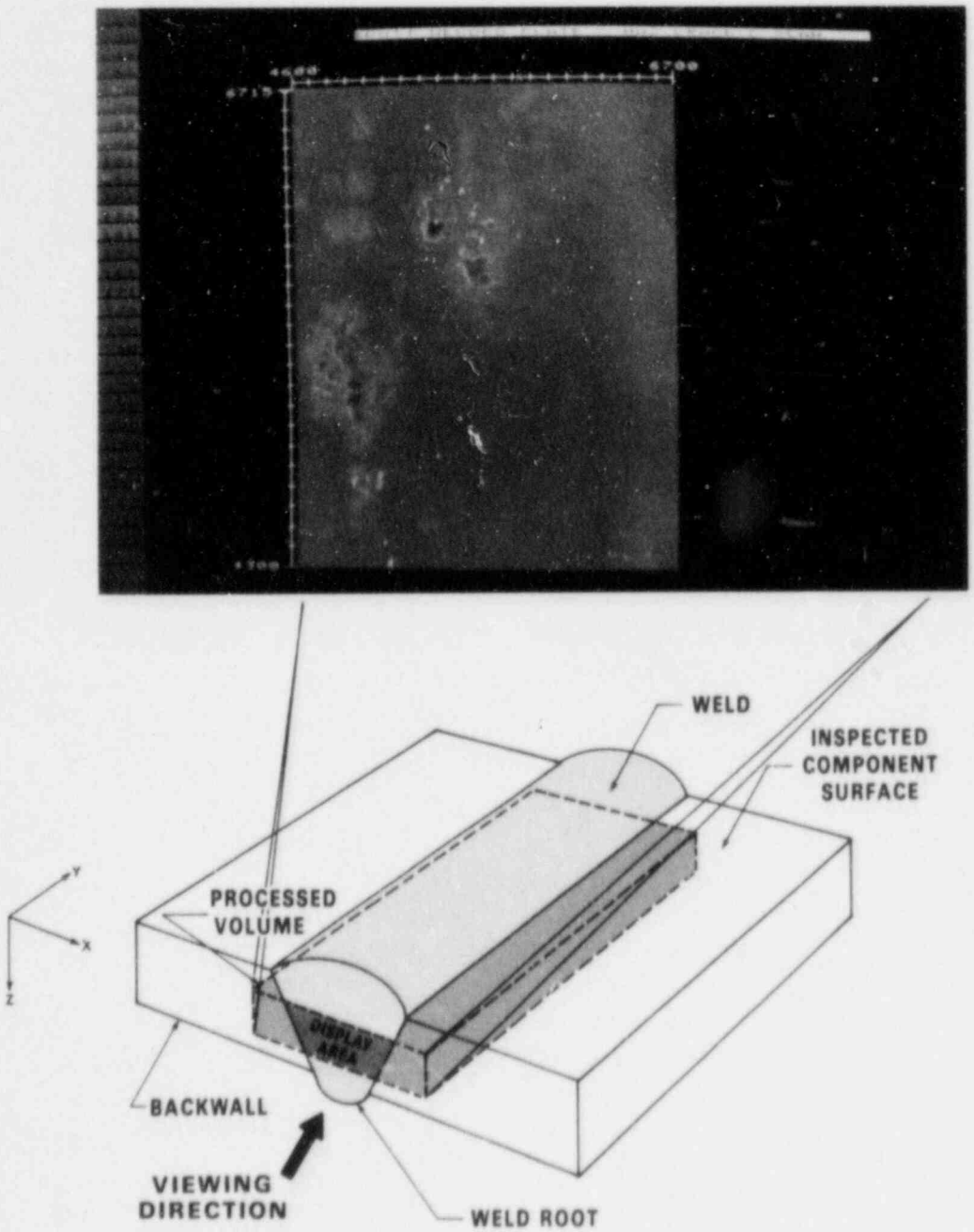

FIGURE 18. BUTT-WELDED CARBON STEEL PLATE SPECIMEN - WELD CRACK/PITTING
(B-Scan View Transverse to Weld)

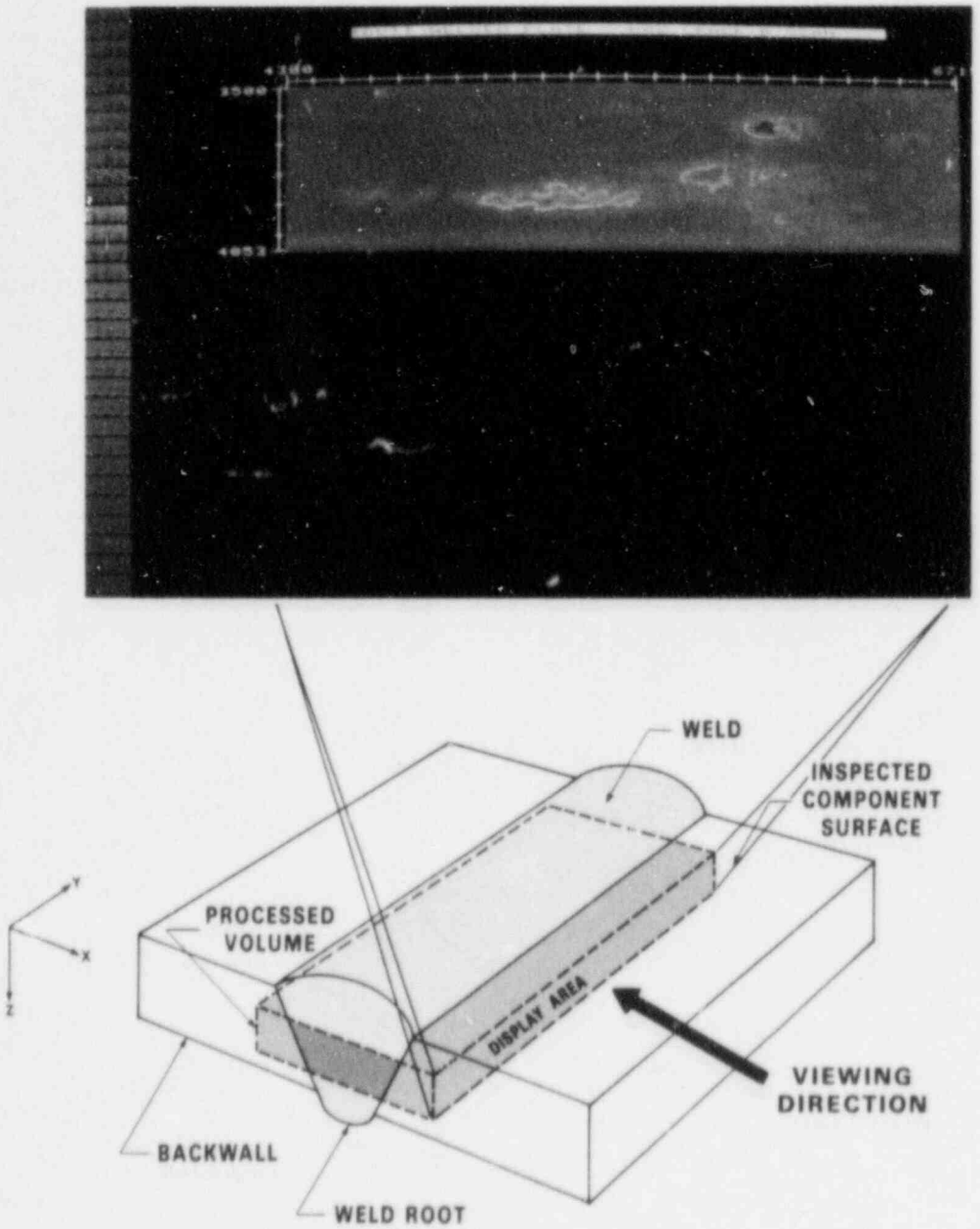

FIGURE 19. BUTT-WELDED CARBON STEEL PLATE SPECIMEN - WELD CRACK/PITTING
(B-Scan View Parallel to Weld)

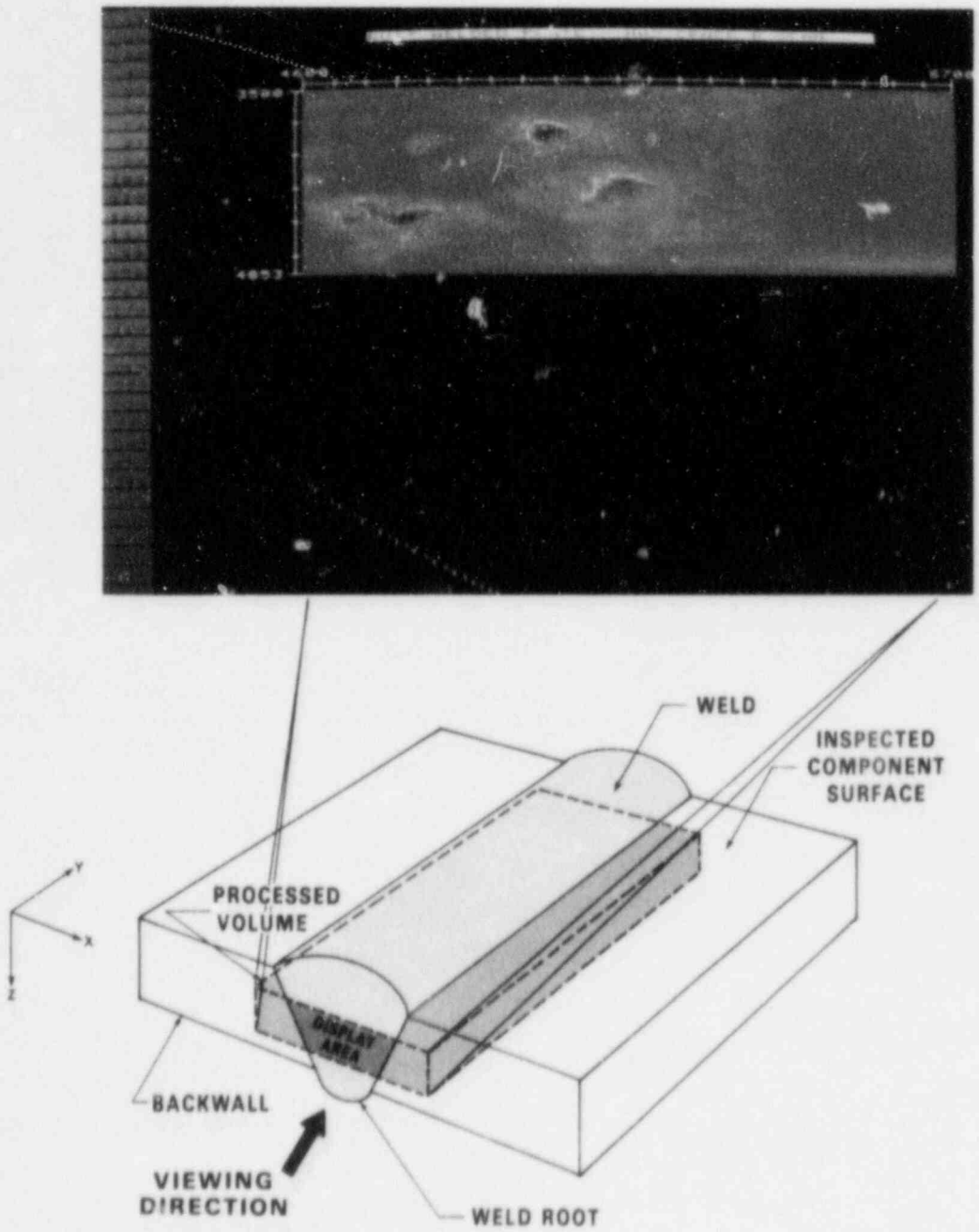

FIGURE 20. BUTT-WELDED CARBON STEEL PLATE SPECIMEN - WELD CRACK/PITTING
(B-Scan View Transverse to Weld)

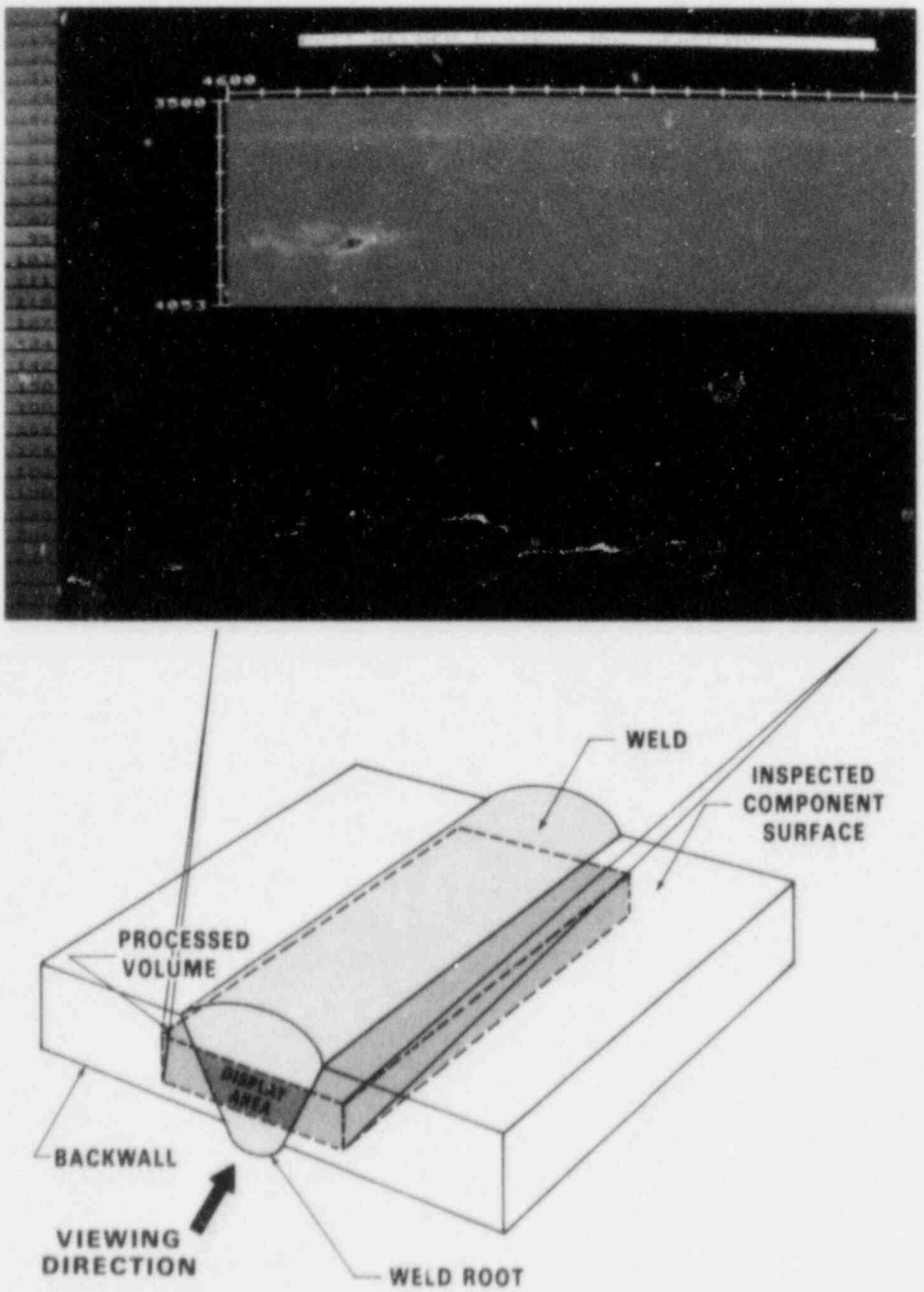

FIGURE 21. BUTT-WELDED CARBON STEEL PLATE SPECIMEN - WELD METAL CRACKING
(B-Scan View Transverse to Weld)

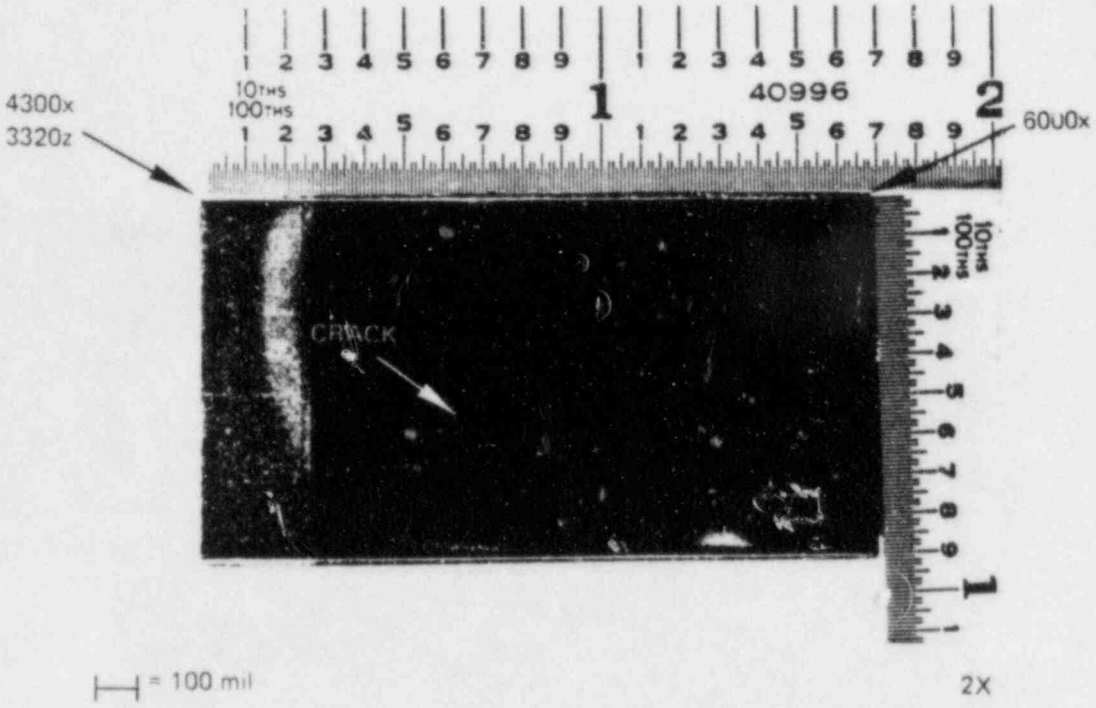

FIGURE 22. BUTT-WELDED CARBON STEEL PLATE - WELD METAL CRACKING AND PITTING (B-scan section at y=5100)

Sectioned specimen piece showing coordinate and axis labels corresponding to the imaged volume. The crack is approximately 70 mils (1.80 mm) across and located entirely within the weld metal. Through-wall depths can be determined by subtracting the front surface location [3182 mils (80.8 mm)] from any z-axis location.

Another B-scan (parallel to the weld) presentation, obtained by sawing through the crack parallel to the weld, is shown in Figures 23 and 24. This reveals that a combination of porosity and cracking make up the extent of this flaw. The porosity was composed of numerous small 0.015-inch (0.4-mm) diameter pits separated from adjacent pits by 0.01 to 0.03 inch (0.5 to 0.76 mm). Therefore, this interlaced-flaw structure composed of cracks and pits was imaged as a single continuous reflecting surface.

One of the two isolated imaged flaws was located and is shown using a B-scan (transverse to the weld) presentation in Figures 25 and 26. This flaw was made up of larger pits 0.04 inch (1 mm) in diameter separated by 0.01 inch (0.25 mm) and was, therefore, imaged as one reflecting surface. The second isolated imaged flaw was destroyed during the sectioning process. The weld flaw fabrication process used to create this flaw did not result in the desired heat-affected-zone cracking. Instead, only a small amount of weld metal cracking and porosity was introduced in the weld metal region.

Sizing predictions for the x-axis lengths of both the crack and isolated larger porosity are shown in Figure 27. Sizes determined by measuring that portion of the flaw surface estimated to be acoustically reflective are also annotated in the figure caption. Evaluation of the z-axis through-wall locations using the depth-spread function indicates a resolution capability of at least 1 wavelength using an 8 dB down threshold.

5.3.2 Radiography

None of the flaws present in this region of the test specimen was visible on the radiographs.

5.3.3 Manual UT Examination Results

No recordable indications (20 percent DAC or above) were noted in this flaw region using 0-, 45-, and 60-degree inspection angles.

5.4 Heat-Affected Zone-to-Base Metal Cracking Region

The imaged heat-affected zone-to-base metal cracking region contained within the butt-welded carbon steel plate is shown in Figures 28, 29 and 30. These three figures are compressed view presentations and, therefore, show a composite of the flaw viewed from the corresponding axis projection. Information defining the location, size, and shape relative to the entire imaged volume can be obtained from these views.

5.4.1 Destructive Sectioning

Destructive sectioning was performed by sawing the specimen at locations defined by studying the SAFT UT images. Four destructive sections are shown which represent B-scan-type (transverse to weld) viewing orientations. Several horizontally oriented and one vertically oriented crack were located during destructive sectioning. Destructive sections at three areas of the largest horizontally oriented crack are shown in Figures 31 through 36. This crack exists in the weld fusion area and extends into both the weld and base metal regions. A second, but smaller, horizontally oriented crack is shown in Figures 37 and 38. This crack exists entirely in the base metal and

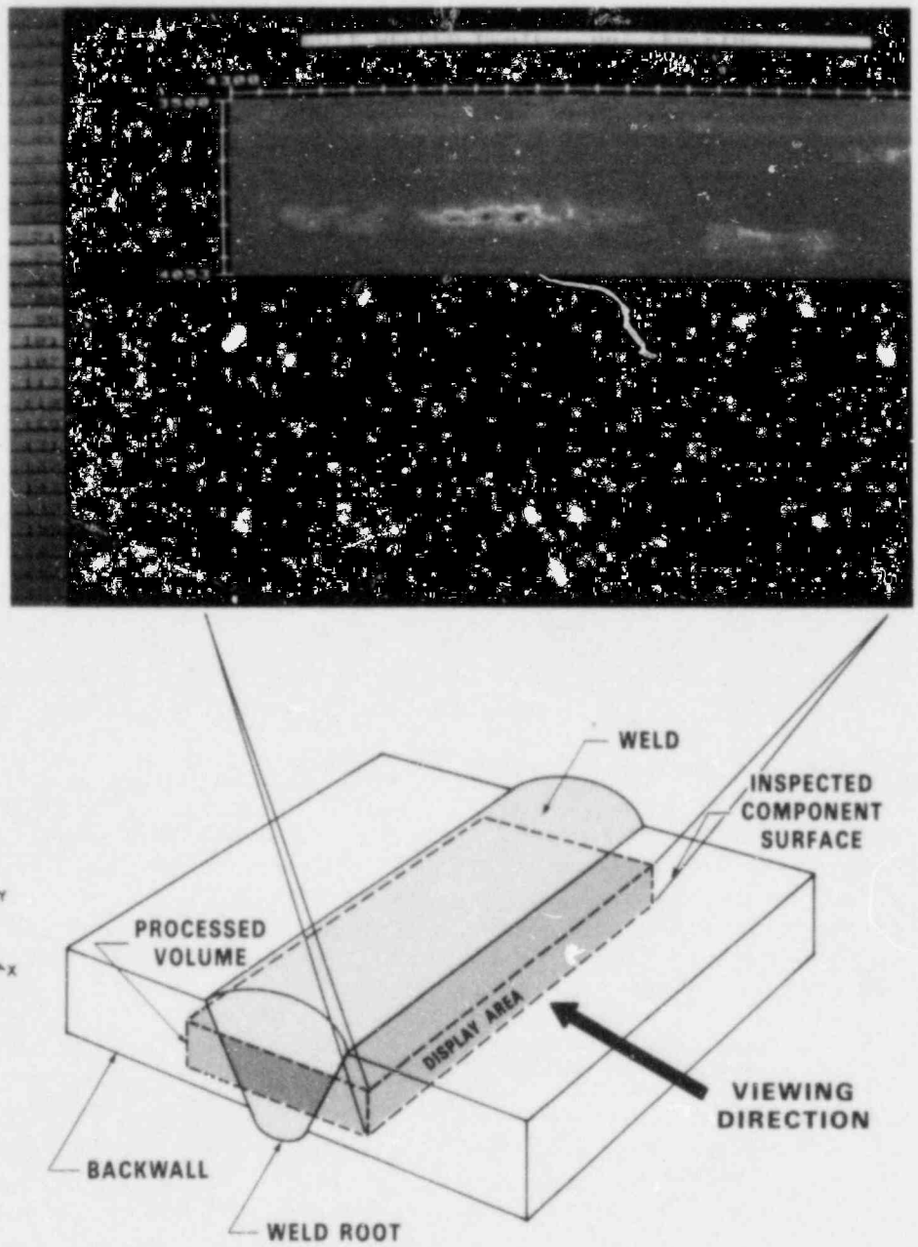

FIGURE 23. BUTT-WELDED CARBON STEEL PLATE SPECIMEN - WELD METAL CRACKING/PITTING
(B-Scan View Parallel to Weld)

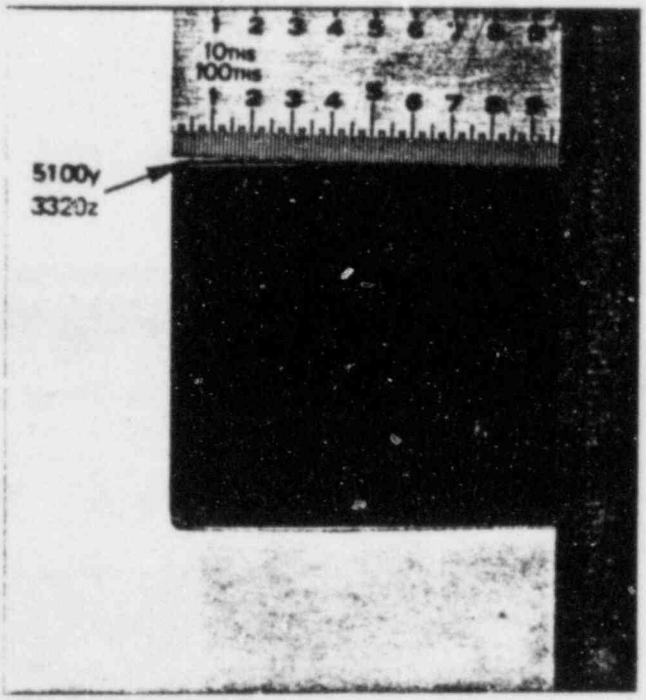

FIGURE 24. BUTT-WELDED CARBON STEEL PLATE - WELD METAL CRACKING AND PITTING (B-scan section at y=4950)

Sectioned specimen piece showing coordinate and axis labels corresponding to the imaged volume. This section was obtained by cutting the crack shown in the section of Figure 20 parallel to the weld. The flaw was then found to be composed of a series of closely spaced small pits and connected cracks. A second flaw located ≈600 mils (15 mm) from the larger flaw can be seen in this view. It also was found to consist of small pits and cracks. Through-wall depths can be determined by subtracting the front surface location [3182 mils (80.8 mm)] from any z-axis location.

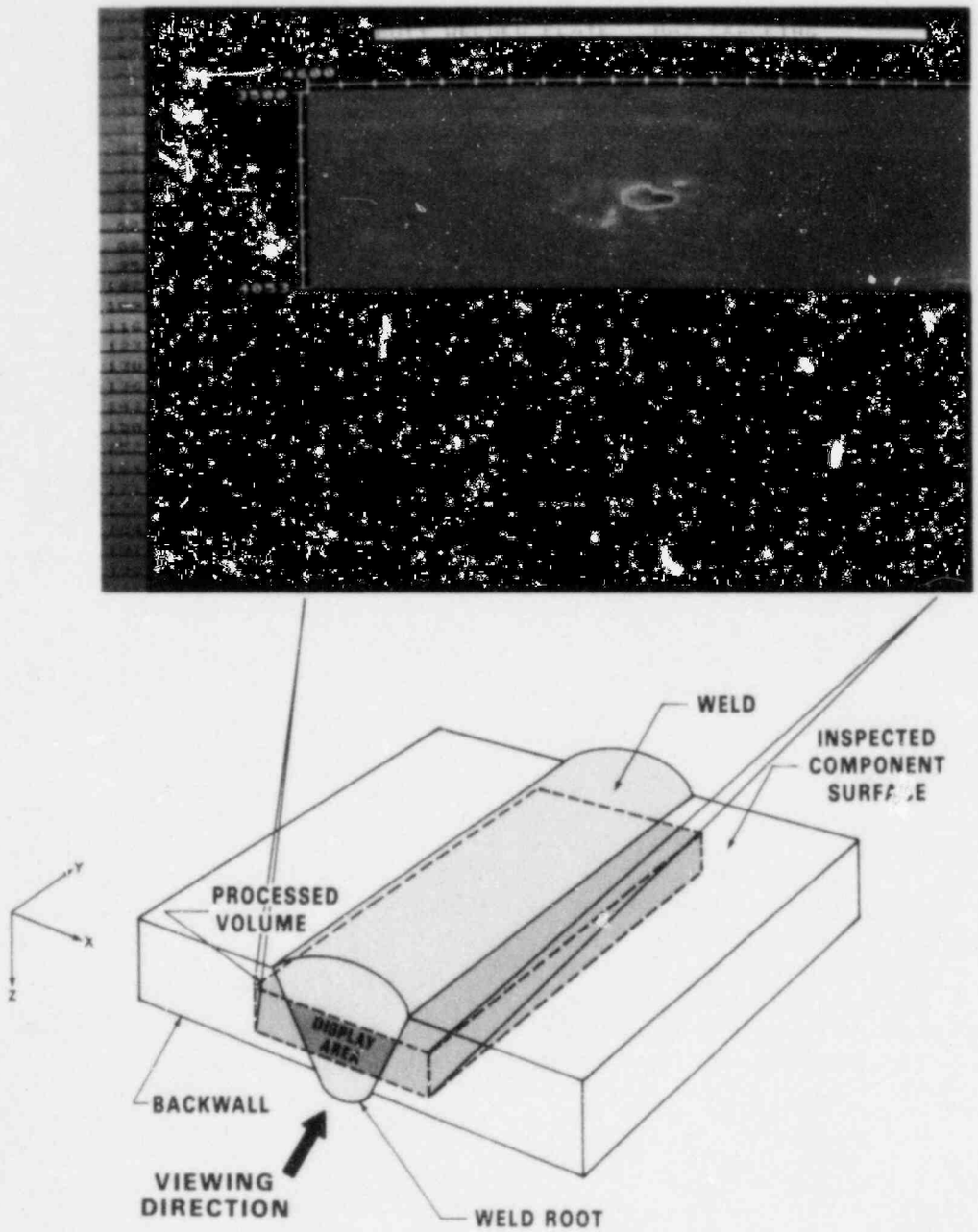

FIGURE 25. BUTT-WELDED CARBON STEEL PLATE SPECIMEN - WELD METAL PITTING
(8-Scan View Transverse to Weld)

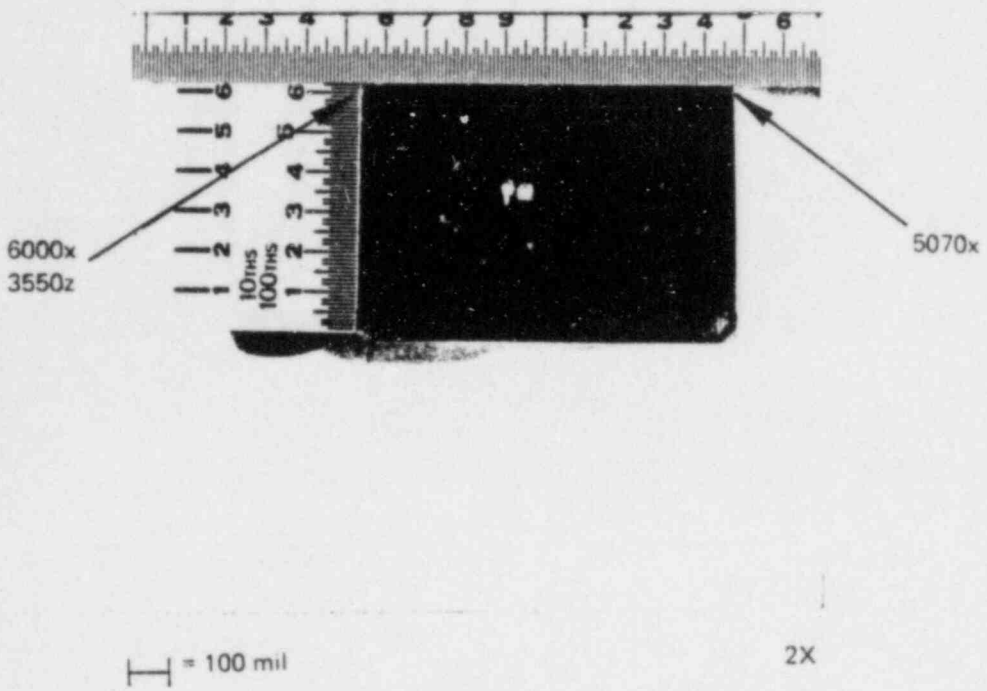

FIGURE 26. BUTT-WELDED CARBON STEEL PLATE - WELD METAL CRACKING AND PITTING (B-scan section at y≈5700)

Sectioned specimen piece showing coordinate and axis labels corresponding to the imaged volume. This isolated flaw was found to consist of several larger pits [≈40 mils (1.0 mm) diameter] separated by 10 mils (0.25 mm) and was, therefore, imaged as a single reflector. Through-wall depths can be determined by subtracting the front surface location [3182 mils (80.8 mm)] from any z-axis location.

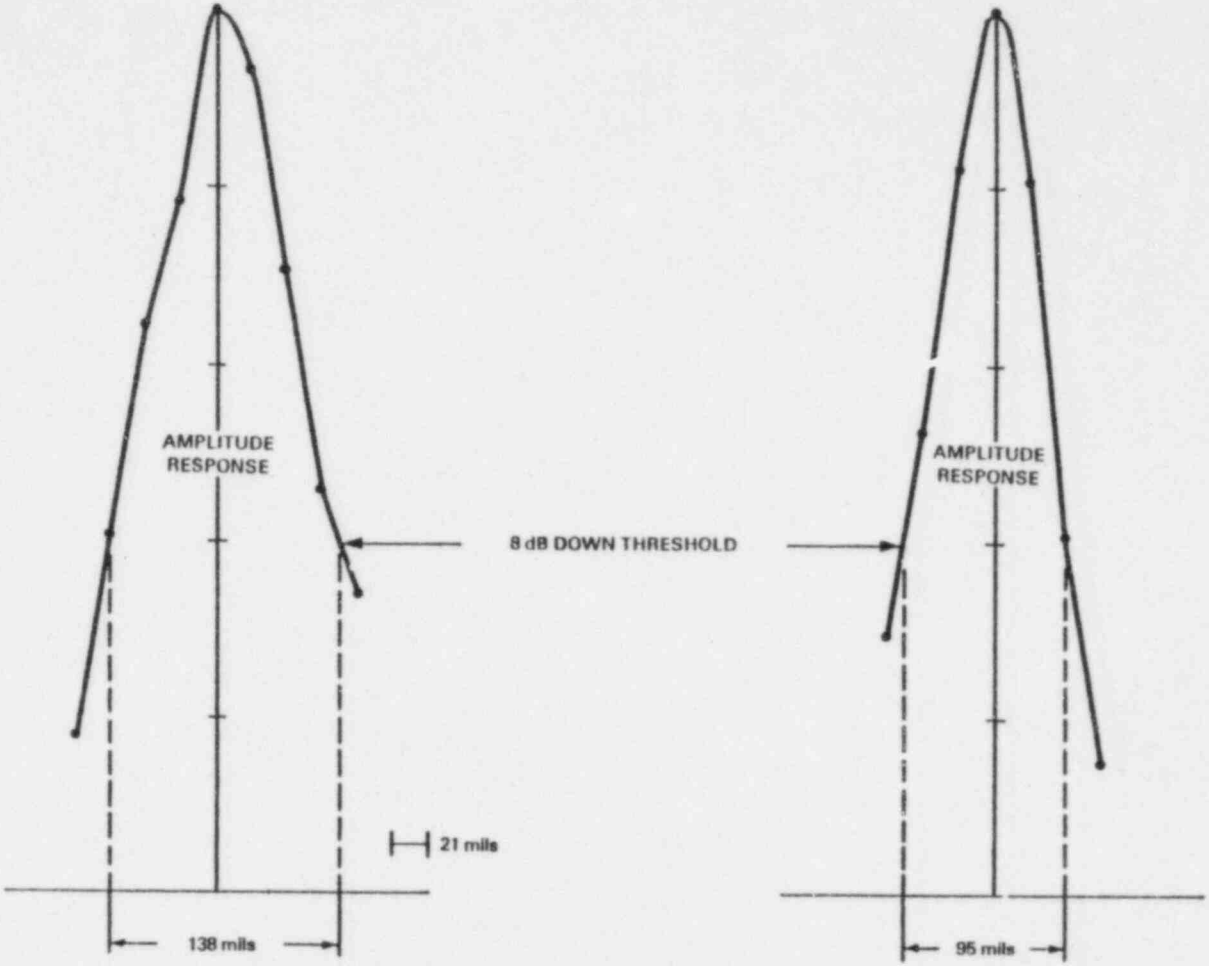

(a) X-Axis Length of Pitting Using Data at Y = 5750, Z = 3780, Measured Size = 75 mils

(b) X-Axis Length of Cracking Using Data at Y = 5050, Z = 3890, Measured Size = 70 mils

FIGURE 27. SIZE PREDICTIONS USING THE SURFACE-SPREAD FUNCTION: BUTT-WELDED CARBON STEEL PLATE - BASE METAL CRACKING AND PITTING REGION

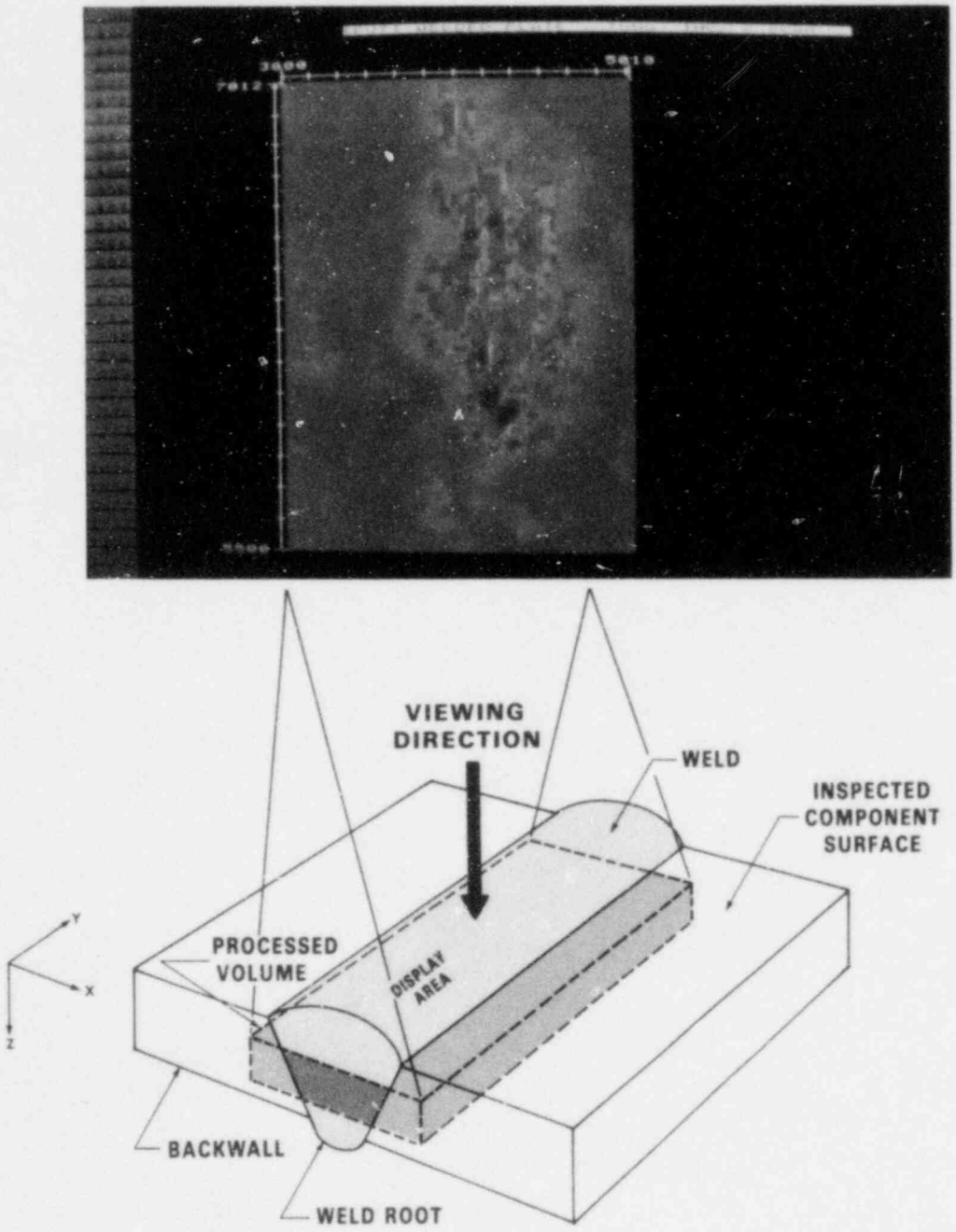

FIGURE 28. BUTT-WELDED CARBON STEEL PLATE SPECIMEN - HEAT-AFFECTED ZONE-TO-BASE METAL CRACKING
(C-Scan View)

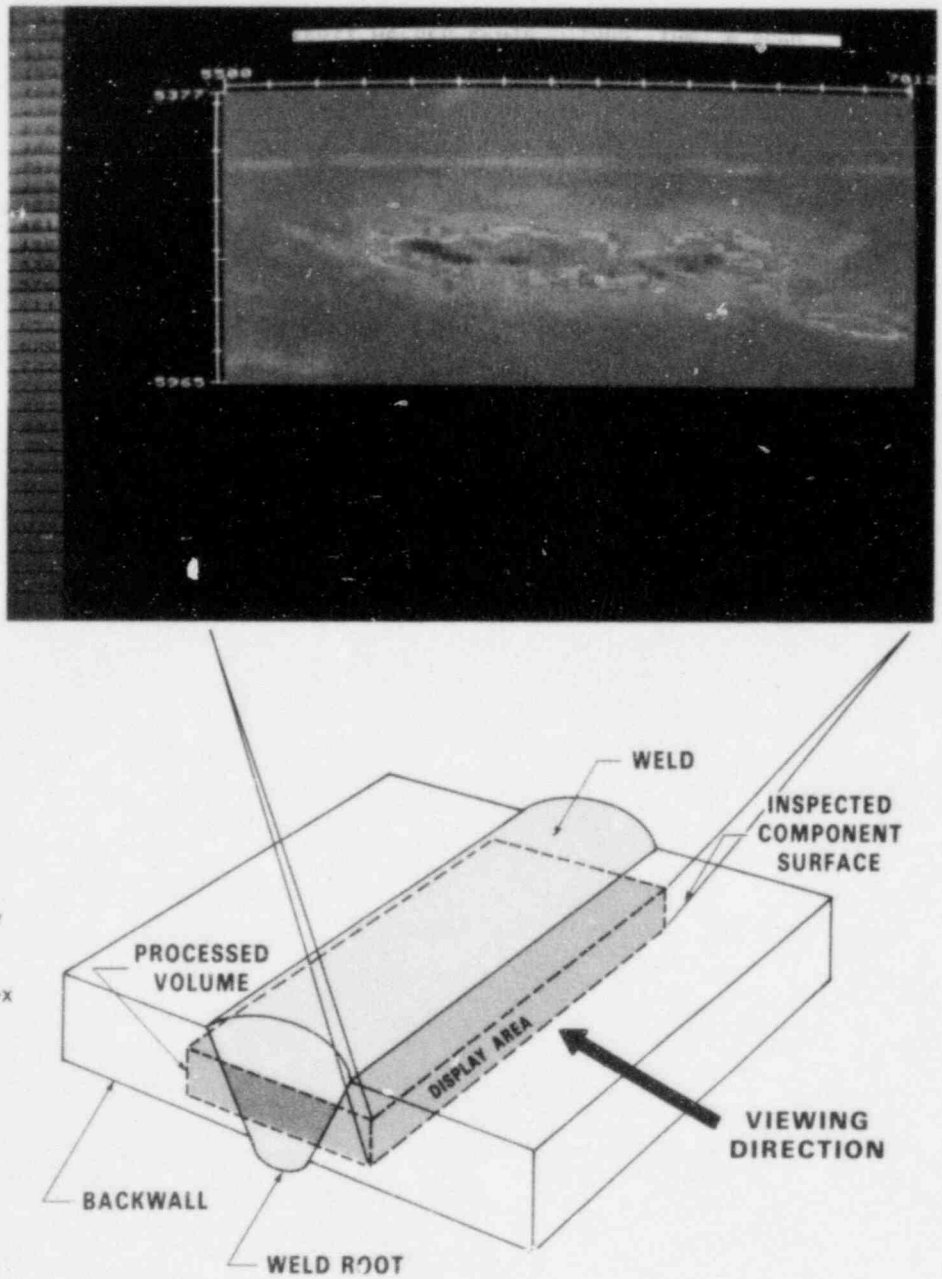

FIGURE 29. BUTT-WELDED CARBON STEEL PLATE SPECIMEN - HEAT-AFFECTED ZONE-TO-BASE METAL CRACKING
(B-Scan View Parallel to Weld)

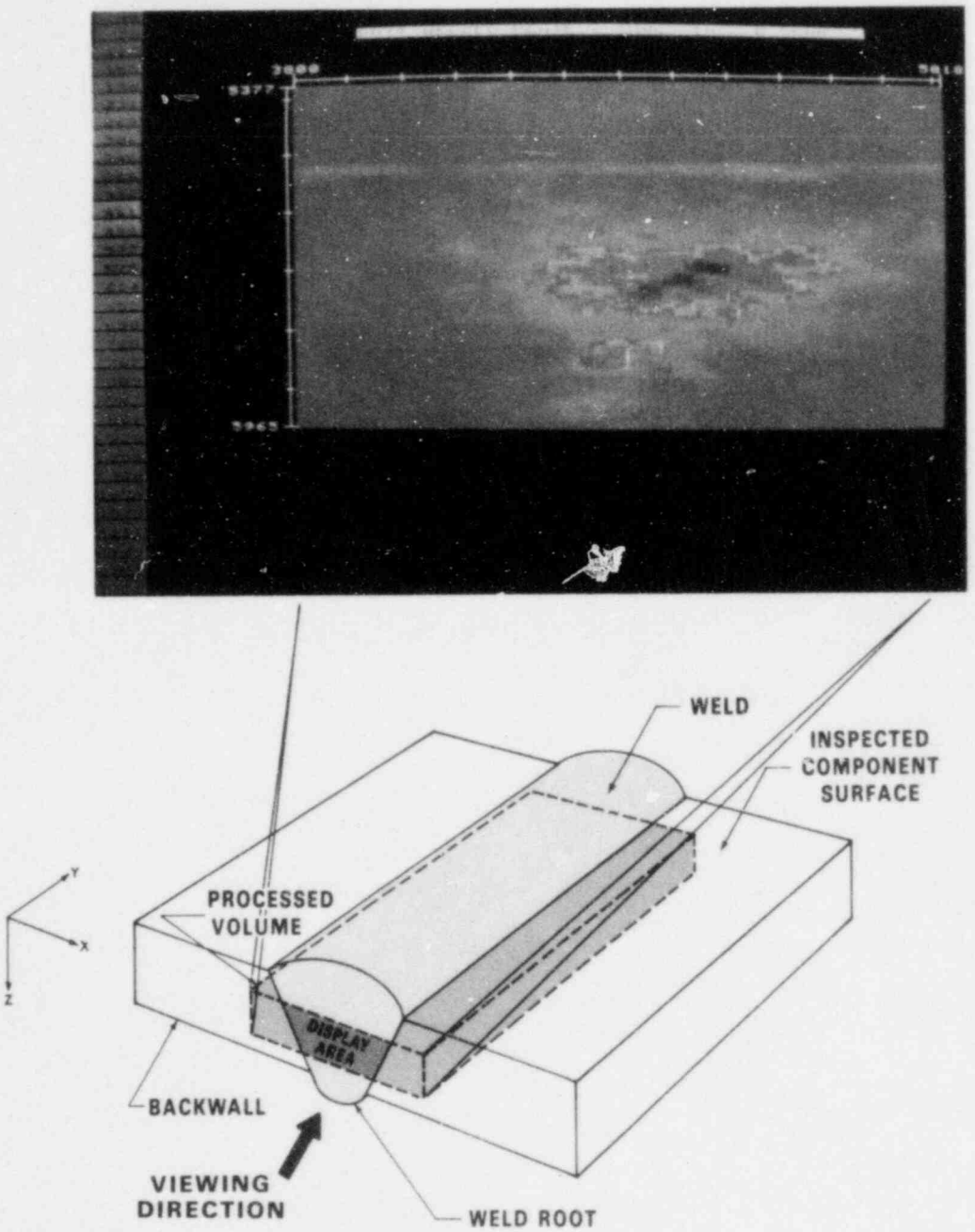

FIGURE 30. BUTT-WELDED CARBON STEEL PLATE SPECIMEN - HEAT-AFFECTED ZONE-TO-BASE METAL CRACKING
(B-Scan View Transverse to Weld)

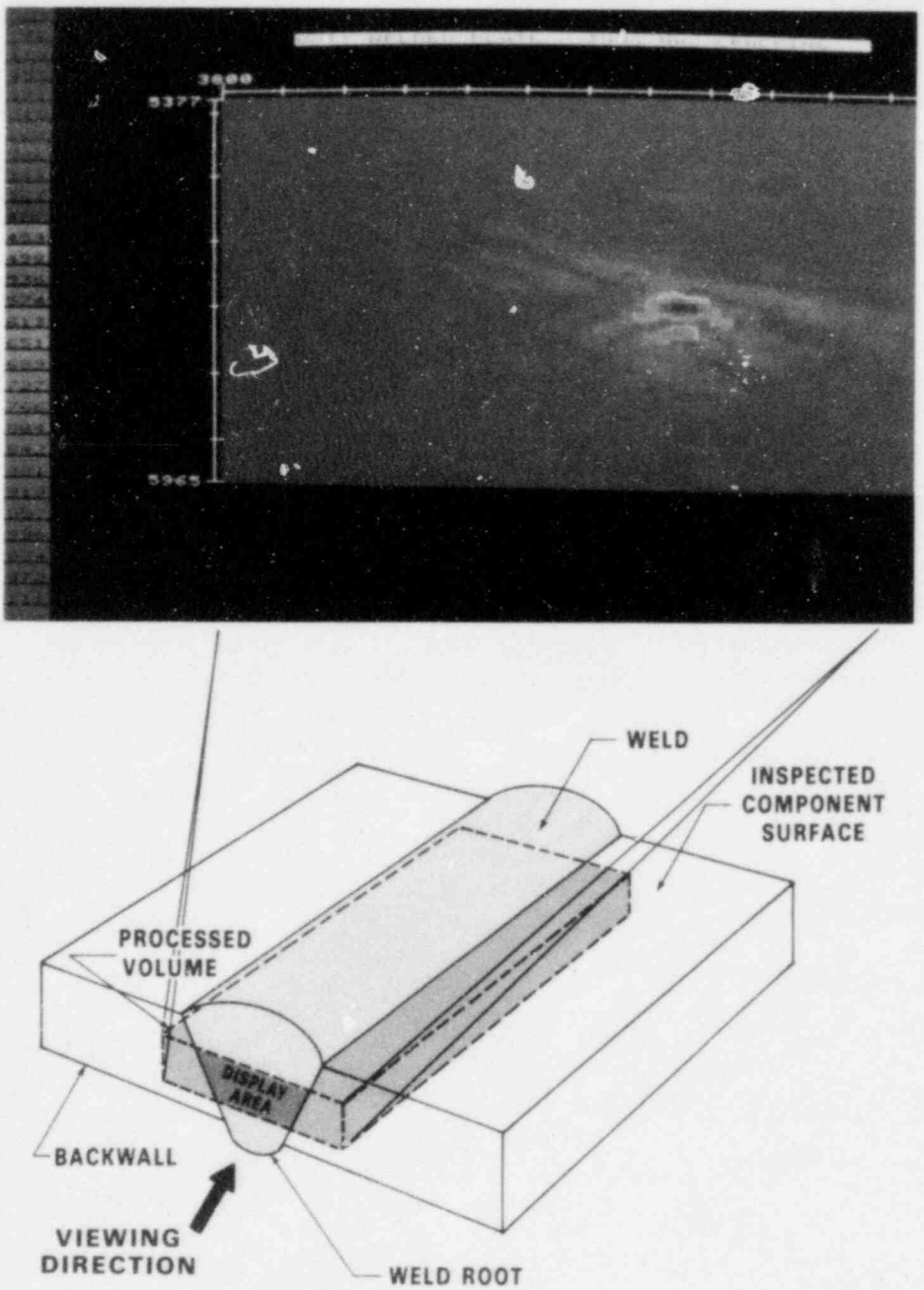

FIGURE 31. BUTT-WELDED CARBON STEEL PLATE SPECIMEN - HEAT-AFFECTED ZONE-TO-BASE METAL CRACKING
(B-Scan View Transverse to Weld)

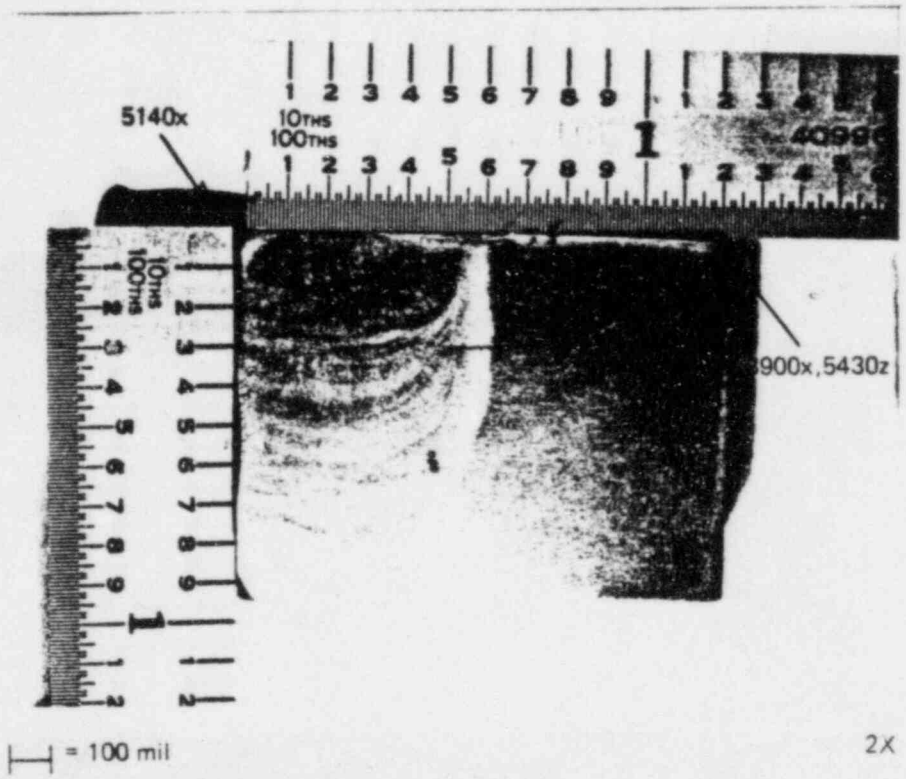

FIGURE 32. BUTT-WELDED CARBON STEEL PLATE - HEAT-AFFECTED ZONE-TO-BASE METAL CRACKING (B-scan section at y=6050)

Sectioned specimen piece showing coordinate and axis labels corresponding to the imaged volume. The sectioned surface has been etched to show the fusion line. Note that the x-axis positions increase from right to left instead of left to right. This is caused by viewing the slice while looking in the decreasing y-axis direction. The small vertically oriented crack is outside the image volume. Through-wall depths can be determined by subtracting the front surface location [3164 mils (80.4 mm)] from any z-axis location.